UNIVERSITAT POLITÈCNICA DE CATALUNYA
BARCELONATECH

Signal waveform for a modem for Satellite Communications

A Degree Thesis

Submitted to the Faculty of the

Escola Tècnica d'Enginyeria de Telecomunicació de Barcelona

Universitat Politècnica de Catalunya

by

Ossama Armas Mousa

In partial fulfilment

of the requirements for the degree in

Science and Technologies of Telecommunication Engineering

Advisor: Francesc Rey Micolau

Barcelona, January 2020

Abstract

At present, the main frequency bands addressed for deep-space missions are being overpopulated. Due to this rapid congestion, the CCSDS standard proposes a follow-up of recommendations based on the simultaneous transmission of telemetry and ranging in order to make much more efficient use of the spectrum and approach high rates transmission.

The purpose of this project is to verify and demonstrate through simulations the correct operation and target achievement of the system, in addition to propose a more versatile alternative receiver.

Finally, a ranging cancellation system will be applied based on the new recommendation of the standard to overcome the main disadvantages of the system and give rise to a more reliable and robust reception system.

Resum

En l'actualitat, les principals bandes freqüencials destinades a missions d'espai profund s'estan superpoblat. A causa d'aquesta ràpida congestió, l'estàndard CCSDS proposa un seguit de recomanacions basades en la transmissió simultània de Telemetria i Ranging amb tal de fer un ús molt més eficient de l'espectre i apropar-se a transmissions d'alta velocitat.

El propòsit d'aquest projecte és verificar i demostrar mitjançant simulacions el funcionament correcte i l'assoliment de l'objectiu del sistema, a més de proposar un receptor alternatiu més versàtil.

Finalment, es passarà a aplicar un sistema de cancel·lació de Ranging basat en la nova recomanació de l'estàndard per superar els principals desavantatges del sistema i donar lloc a una recepció més fiable i robusta.

Resumen

En la actualidad, las principales bandas frecuenciales destinadas a misiones de espacio profundo se están superpoblando. Debido a esta rápida congestión, el estándar CCSDS propone un seguido de recomendaciones basadas en la transmisión simultanea de telemetría y ranging con tal de hacer un uso mucho más eficiente del espectro y acercarse a las transmisiones de alta velocidad.

El propósito de este proyecto es verificar y demostrar mediante simulaciones el correcto funcionamiento y objetivo alcanzado del sistema, además de proponer un receptor alternativo más versátil.

Finalmente, se pasará a aplicar un sistema de cancelación de ranging basado en la nueva recomendación del estándar para superar las principales desventajas del sistema y dar lugar a un sistema de recepción más robusto y fiable.

Acknowledgements

I want to express my most sincere gratitude to my dear family, friends and all those people who supported me and continue to do so. All of them essential pillars in fulfilling this goal in my life. Finally, thanks to Francesc Rey for guiding me during the project and for always being available.

“An investment in knowledge pays the best interest”

– Benjamin Franklin

Revision history and approval record

Revision	Date	Purpose
0	06/12/2019	Document creation
1	17/12/2019	Document revision
2	17/01/2020	Document revision

DOCUMENT DISTRIBUTION LIST

Name	e-mail
Ossama Armas Mousa	armas_cena@hotmail.com
Francesc Rey Micolau	francesc.rey@upc.edu

Written by:		Reviewed and approved by:	
Date	06/12/2019	Date	24/01/2020
Name	Ossama Armas Mousa	Name	Francesc Rey Micolau
Position	Project Author	Position	Project Supervisor

Table of contents

List of Figures

List of Tables

1. Introduction

1.1. Statement of Purpose

The purpose of this project consists, on the one hand, in the development, implementation and posterior analysis of a downlink communication scheme, both transmitter and receiver, which are based on the simultaneous transmission of a Gaussian Minimum Shift Keying shaped telemetry signal (TM) and a pseudo-noise ranging signal (RG), both combined through a phase modulator for its subsequent transmission.

On the other, it will serve to define a path towards the use of downlink systems with very high rated telemetry in the future, emphasizing into deep space missions and Ka [26.5 - 40] GHz frequency band.

Development of the project will be based on the data and systems recommendations created by the Consultative Committee for Space Data Systems **(CCSDS)** whose standards have already been used by more than 900 space missions and its new added recently standard about ranging cancellation **[1].**

Regarding the objectives of this work, these are:

1. Implement a transmitter based on a combination of telemetry and ranging signal.

2. Study the impact of adding the ranging signal on the telemetry at different data rates ratio defined by the standard.

3. Develop and implement a receiver able to demodulate telemetry and ranging with a good performance in terms of BER and ranging acquisition.

4. Enhance the system through the implementation of a ranging cancellation system and study the results and performance.

5. Describe future paths towards the transmission of high rate telemetry.

1.2. Methods and Procedures

This Project is based on an idea proposed by the European Space Agency (ESA), on which describes the fact that future space missions will require high data rates as well as an efficient frequency band usage and hence, appears the necessity of new communication system and technics adapted to that rate increment. In that way, CCSDS books based on simultaneous transmission of telemetry and ranging have been used as a guideline to develop the system. In order to validate and analyse the performance and behaviour of the system, it has been simulated through different MATLAB codes, all of these self-developed in order to ensure skills and knowledge acquisition.

1.3. Incidences and Deviations

During the development of the project no critical incidences have happened which could have affected the time plan done and illustrated on the critical review document. Fortunately, problems found during the coding of the receiver had been solved rapidly through analysis of the erroneous results, hence no important deviations have happened.

1.4. Requirements and Specifications

Project's main goal is to study the behaviour of the combined telemetry – ranging signal and the performance of both recommended transmitter and developed receiver in a perfectly synchronized downlink.

As it has been said, this system is developed based on CCSDS recommendations, hence there are certain requirements to be accomplished to ensure the correct operation of the downlink communication system described next.

These are:

- The system must comply with the recommendations specified in **CCSDS 401 – 2.4.22 A & B. [1]**
- Pre-coded GMSK modulation with a bandwidth-time product (B·Ts) of:
  - **0.25** for Category A Missions.
  - **0.5** for Category B Missions.
- Ranging modulation index h_m:
  - **0** to **0.7** rad in step sizes of **0.5**.
- Generation and correlation of both ranging chip sequences **T2B** and **T4B**, according to **[4].**
- The modulated signal spectrum of **GMSK** without **PN** Ranging signal shall be compliant to the **ECSS** emission mask **(Figure 6-5 of ECSS) [2].**
- Ground receiver should be able to demodulate the **TM** of a **GMSK** signal without ranging cancellation **[3].**
- Ground receiver should be able to demodulate TM of combined GMSK + PN Ranging signal with and without ranging cancellation according to **CCSDS 401 – 2.4.22 A & B [2].**
- The ground breadboard shall be able to demodulate the RG signal of a combined GMSK + PN RG signal **[3]**, with and without ranging cancellation, according to CCSDS 2.4.22 A & B **[1].**

1.5. Organization of the thesis

The purpose of this section is to describe the project's organization which is divided into 5 chapters.

On the first chapter, a basic introduction of the project has been done, highlighting the main goals of the project as well as a scope describing the main objective.

Second chapter is focused into a detailed explanation of all the theoretical background used to develop the whole project. In addition, introduces the origins of the problem from which this project arises and all the restrictions and recommendations imposed by CCSDS standard, on which this project is subjected.

On the third chapter, development of the communication system based on the simultaneous transmission of telemetry and ranging will be presented. From the design of the transmitter to the receiver, a detailed breakdown of the different parts of the system are done in order to understand the different factors and their respective impact. Technics such as Laurent Expansion, Ranging Cancellation and ranging codes attributes are illustrated.

The fourth chapter is devoted to present the results of the system developed in terms of bit error probability (BER) for the telemetry signal and probability of acquisition of the ranging sequence. It will show system behaviour and improvements done by the implementation of the ranging cancellation system as well as the proposed GMSK receiver based on Viterbi Algorithm and Laurent's Decomposition.

Finally, on the fifth chapter, the project conclusions are drawn and a possible future line of work is considered based on the results obtained.

2. State of the art of the technology used or applied in this thesis:

2.1. Project Background

Before introducing ourselves to detailed theoretical aspects we will raise the main problem from which this project arises.

Several upcoming missions will focus on conducting scientific experiments and deep space exploration requiring the improvement of many technological aspects to overcome limitations on establishing reliable and solid communication links, meeting the requirements imposed by each mission.

An important issue to address is the electromagnetic spectrum. Currently there are a certain number of primary space research service (SRS) allocations that are used for telecommand, telemetry and radiometric data collection.

These allocations given in Table 1 below, are designed specifically for only deep space missions or for both deep space missions and non-deep space **[5]**.

Table 1: Allocated Frequency Bands

Band Designation	Deep Space Bands		Near Earth Bands	
	Uplink Earth to Space	Downlink Space to Earth	Uplink Earth to Space	Downlink Space to Earth
S Band	2110 – 2120 MHz	2290 – 2300 MHz	2025 – 2110 MHz	2200 – 2290 MHz
X Band	7145 – 7190 MHz	8400 – 8450 MHz	7190 – 7235 MHz	8450 – 8500 MHz
K Band	--	--	--	25 500 MHz
Ka Band	34.2 – 34.7 GHz	31.8 – 32.3 GHz	--	--

Since the focus of this project is on the Space to Earth link i.e. downlink, it is interesting to describe the current status of the bands presented above.

Increasing congestion of S Band allocation and the addition of allocations for incompatible services (e.g., IMT-2000) have restricted future operations in the 2 GHz deep space band. Accordingly, the Science Mission Directorate is recommending that use of the 2 GHz deep space band be limited to radio science and in-situ communications.

Next, we have the X downlink band segment **8400 - 8450 MHz** (Space to Earth) which is actually overpopulated since it is being used from the beginning by all deep space missions and that's a problem for future space missions that resort to this frequency band due to possible interference issues.

As a result of this congestion, it is beginning to transition towards the use of higher and not so populated frequency bands such as the Ka band that ranges from **31.8 to 32.3 GHz.**

2.2. Spectrum Requirements for Deep-space missions

The number of future space missions are expected to increase greatly as well as the telemetry rates to transmit the generated data to the ground station, so the needed spectrum to support the space to earth link is also expected to increase rapidly within the next years.

One of the reasons of the rate increment is that currently the on-board instruments responsible for conducting experiments and measurements increasingly need higher rates perhaps exceeding hundreds of megabits per second, as it's shown in Table 2.

Table 2: On Board Instruments data rate requirements

User Spacecraft	Instrument	Data rate (Mbit/s)
Robotic rovers	Surface radar Hyperspectral imaging	100 150 - 600
Science orbiters	Orbiting radar Hyperspectral imaging	100 150 - 600
Human transports	Hyperspectral imaging	150 - 600

An important aspect to consider is that the return of scientific data from deep space is limited to the capacity of the downlink, since generally only a fraction of the one that is capable of collecting is sent.

Furthermore, deep space missions may take months and even years to reach their destination, but they have a fairly limited time that can vary from days to a few weeks to study their objective and therefore the bit-rate increase is essential for such as transmitting the greatest amount of information in the shortest possible time, this being an advance that would have a positive impact both economically and scientifically.

2.3. CCSDS Standard and SFCG spectral Mask

As discussed in previous points, the frequency bands are rapidly saturating. To avoid this rapid congestion and its consequent interference problems, the CCSDS has issued recommendations based on compact and spectrally efficient modulations, in addition to technics for high-rate transmissions, not only to make the most efficient use of the band but to have access to inter- agency cross-support capability which implies some design standardization given by CCSDS recommendations such as RF and modulation standards for Earth Stations and spacecrafts **[3]**.

In this context, CCSDS has recommended a system capable of simultaneously transmitting telemetry at high rates and ranging in the X-band segment indicated in Table 1.

This system transmits telemetry **(TM)** through a standardized **GMSK** modulator and a ranging signal generated from pseudo-random noise **(PN)** sequences. Both signals are combined through a phase modulator, so that the ranging signal becomes an additional phase shift within the entire signal **[2].**

Specifically, the project must follow the recommendations established in points 2.4.22A and 2.4.22B of the standard **[1]** regarding the generation and modelling of said signals, followed by parameters with a defined characterization range and proposals for transmission - reception schemes and applicable techniques.

As a last aspect, Space Frequency Coordination Group **(SFCG)** adopted a spectral mask that precludes the use of a number of classical modulations schemes for missions launched after 2002 **[2]**. This spectral mask provides guidance on the maximum allowable bandwidth as a function of data rates for Space to Earth links on the frequency bands portions mentioned previously.

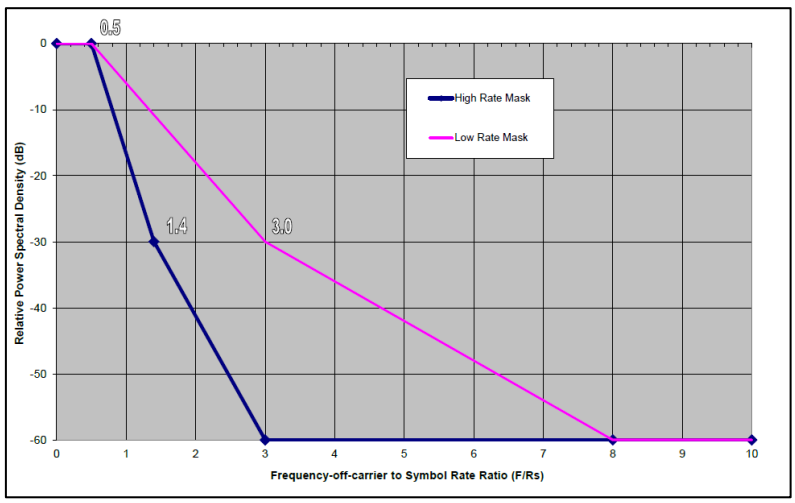

Figure 2-1: SFCG Mask [5]

While the spectral mask under recommendation described in Fig. 2-1 does not address the ranging signal but only to be compliant with the TM modulation, it's used to provide an indication of how good the selected simultaneous telemetry and ranging transmission can be from a spectral management point of view.

After having briefly introduced the CCSDS standard and what it implies, we reach a key point in the state of the art in which it is important to introduce aspects as relevant as Continuous Phase Modulations **(CPM)** and therefore the GMSK that proposes the standard as well as the ranging.

2.4. Signal for data transmission

Digital communication generally must overcome various factors such as fading, path loss and other characteristic channel factors. Because of this, there's an effort behind to maintain a certain level of power in reception and therefore to opt for the use of amplifiers, such as, traveling-wave tube amplifiers **(TWTA)** and solid-state power amplifiers **(SSPAs).**

The problem arises when these amplifiers work in its saturation zone. The latter causes that when the modulations go through these non-linearities, distortions occur in the AM - AM and AM - PM relationships resulting in changes in the amplitude and phase of the symbols. **[6]**

Because of this, modulations that transmit information via their amplitude, e.g., quadrature amplitude modulation **(QAM)**, and therefore need a linear amplifying characteristic, are not suitable for its use.

A second effect to take into account is the spectral regrowth (see Fig. 2-2), which causes spurs outside the spectral band. As it is mentioned before, a spectral mask imposed by regulating agencies must be complied with, therefore, the modulation must be designed in order to fall under it and keep the spectral spreading minimum.

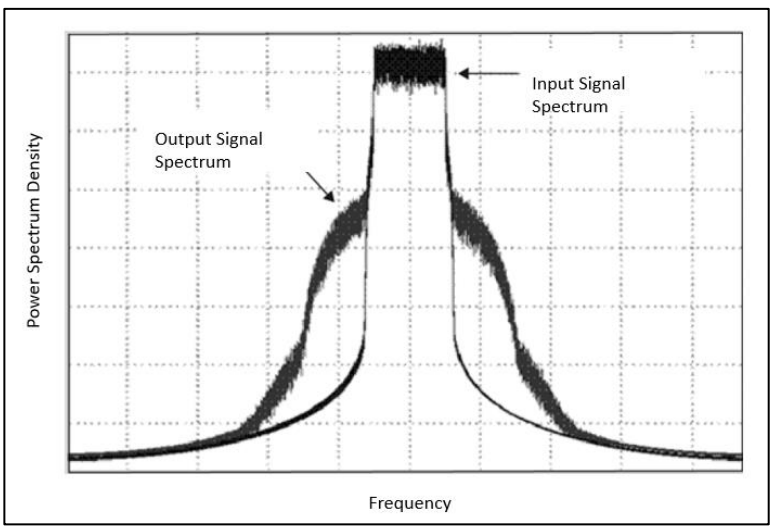

Figure 4-2: Spectral Regrowth

In front of these distortions it is necessary to set two important requirements for the modulations.

These are:

1. Constant envelope: As we have seen, when the signal is constant, nonlinear amplifiers do not distort information symbols. Therefore, modulations with this property will be sought.

2. Continuous phase: In order to achieve modulations with reduced bandwidth, apart from the constant envelope requirement, we will require that the signal does not have sudden instantaneous changes (discontinuities), which will result in a widening of the spectrum.

Both restrictions guide us to define the next key element which are the Continuous Phase Modulations.

2.4.1. C.P.M Model and GMSK

A continuous phase modulation is a constant envelope modulation whose structure is as follows:

$$S_{CPM}(t) = A_c * \cos(2\pi f_c t + \varphi(t,\alpha) + \varphi_o) \quad (1)$$

Where $\boldsymbol{A_c}$ is the carrier signal amplitude, $\boldsymbol{f_c}$ is the frequency carrier and $\boldsymbol{\varphi(t,\alpha)}$ the phase modulation.

In order to guarantee continuous phase, we have to impose a restriction defined by**:**

$$\varphi(t,\alpha) = 2\pi \sum_n \alpha_n h\, q(t-nT) \quad (2)$$

Where $\boldsymbol{h}$ defines the modulation index, $\boldsymbol{\alpha_n}$ the i.i.d. binary transmitted symbols and finally $\boldsymbol{q(t)}$ is the pulse which defines how the phase evolves during the transmission. Pulse's attributes, such as shape, are important when shaping the spectrum of the signal.

The implementation of a CPM modulator in which the continuous phase has to be guaranteed can be carried out through an FM modulator, which presenting an integrator at the signal input ensures that this phase is continuous as shown in Fig. 2-3.

In this way it is interesting to present the derivative of the pulse $\boldsymbol{q(t)}$ $(\mathbf{3})$, which will constitute the instantaneous frequency of the modulation.

$$g(t) = \frac{dq(t)}{dt};\ q(t) = \int_{-\infty}^{t} g(\lambda)\, d\lambda \quad (3)$$

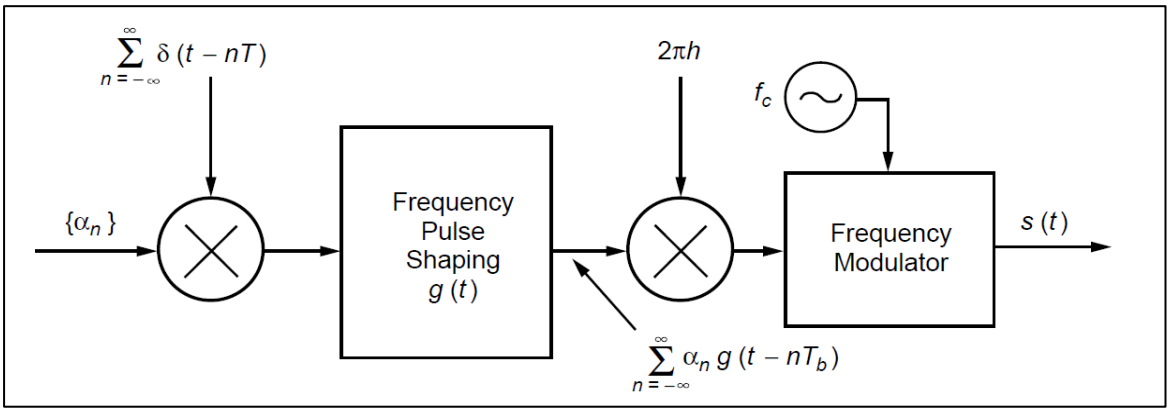

Figure 2-7: C.P.M Modulator [7]

Within the subclasses of CPM, we can find the **GMSK** which is likewise characterized by a pulse $\boldsymbol{g(t)}$ defined by (4), obtained filtering the rectangular frequency pulse characteristic of an **MSK** with a filter having a Gaussian impulse response prior to frequency modulation of the carrier.

As a result, $\boldsymbol{g(t)}$ is defined as the difference of two times-displaced (by Tb) Gaussian probability integrals:

$$g(t) = \frac{1}{2Tb}\left[Q\left(\frac{2\pi BTb}{\sqrt{ln2}} * \left(\frac{t}{Tb} - 1\right)\right) - Q\left(\frac{2\pi BTb}{\sqrt{ln2}} * \left(\frac{t}{Tb}\right)\right)\right], -\infty < t < \infty \qquad (4)$$

One appreciable parameter in (4) is the time-bandwidth product defined through BTb, which will be the configuration parameter of the GMSK. Basically, describes the spectral behaviour of the modulation.

Smaller values of BTb lead to a more compact spectrum but also introduce more ISI and therefore, a degraded error probability performance.

Thus, for a given application, the value of BTb is selected as a compromise between spectral efficiency and BER performance.

Finally, GMSK is mentioned as a partial-response modulation because of the duration of its pulse $g(t)$, whose durations extends beyond a one symbol duration Tb. As a result, the instantaneous phase at a certain moment depends not only on the bit being transmitted but on the previous ones, therefore, it is a modulation with memory.

2.5. Signal for Ranging transmission

One of the key issues of operating a deep-space mission is determining where the satellite is relative to its target. To determine the position, Ranging is used.

Ranging is a procedure through which round-trip light time delay between spacecraft and a ground station is measured.

Several upcoming missions and concretely deep-space missions, need a higher accuracy determination compared to current missions, since further distances will be travelled, so in order to achieve a more precise calculation, regenerative pseudo-noise ranging can be used instead of a regular transparent one.

Regenerative ranging, which is the approach at present used by **CCSDS**, results in a great advantage in front of transparent for low SNR communication links (e.g. deep-space missions) because once received the ranging sequence which had been previously phase modulated into the uplink carrier, the on board receiver demodulates and regenerates it coherently with the uplink, in order to retransmit it in that case to the ground station. Hence, the noise effect on the uplink does not accumulate on the downlink as it would occur in a transparent communication model, thereby increasing the SNR.

The last step at the receiver is to demodulate the signal and correlate the estimated sequence with a locally generated model using a range clock sequence and PN component code to estimate the round-trip light delay. **[4]**

2.5.1. PN Code Structure

Range clock frequency selection, structure and logic combination of PN codes affects the acquisition, precision and ranging probability.

For range measurements where the accuracy is a primary concern, a weighted-voting balanced Tausworthe ($\boldsymbol{T4B}$) code shall be selected. On the other, when the acquisition time is a primary concern a weighted-voting balanced Tausworthe ($\boldsymbol{T2B}$) is used.

Both codes are made of a logical combination of six periodic binary sequences of lengths 2, 7, 11, 15, 19, 23 giving a vote $\upsilon = 4$ or $\upsilon = 2$ to the clock sequence $\boldsymbol{C_1} = (+\mathbf{1}, -\mathbf{1})$, respectively. Fig. 2-4 shows the scheme to generate such sequences:

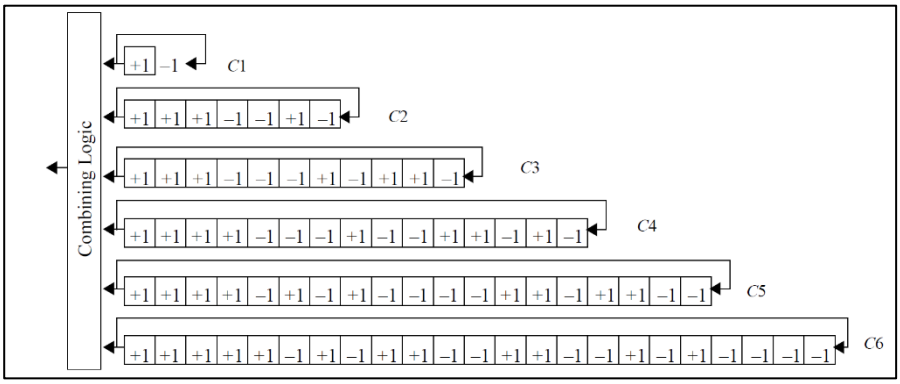

Figure 2-10: PN Code Generator [4]

The output results on a combined sequence C of length $L = 2 \cdot 7 \cdot 11 \cdot 15 \cdot 19 \cdot 23 = 1{,}009{,}470$ chips and depends of the weight selected as:

$$\boldsymbol{C_{T4B}} = Sign(4 * C1 + C2 + C3 + C4 + C5 + C6) \quad (5)$$

$$\boldsymbol{C_{T2B}} = Sign(2 * C1 + C2 + C3 + C4 + C5 + C6) \quad (6)$$

2.5.2. Code Imbalance

An important property of the code, it's that it should exist a balance between the number of +1 and -1 because an imbalance would produce a DC component in the PN Spectrum and that energy can't be used for Ranging.

In order to reduce that imbalance, it's possible to invert components C_3, C_4 and C_6. As a result of inverting these components in (5) and (6) we get:

$$\boldsymbol{C_{T4B}} = Sign(4 * C1 + C2 - C3 - C4 + C5 - C6) \quad (7)$$

$$\boldsymbol{C_{T2B}} = Sign(2 * C1 + C2 - C3 - C4 + C5 - C6) \quad (8)$$

3. Development: Downlink Communication System

3.1. Transmitter

The design of the complete communication system, as indicated in Chapter 2, is derived from CCSDS and specifically on considerations and recommendations found in CCSDS 401 (2.4.22A/B).

Based on the previously outlined points, the standard recommends a transmitter and receiver scheme under design restrictions.

While with the receiver it is quite flexible and gives more degrees of freedom in its implementation, with the transmitter is much more restrictive.

In this section we will study the different parts which constitute the transmitter, starting with the telemetry block, then the ranging and finally the combination of these forming the complete scheme.

3.1.1. Telemetry structure and generation

A telemetry transmitter scheme under these considerations is shown in Fig. 3-1.

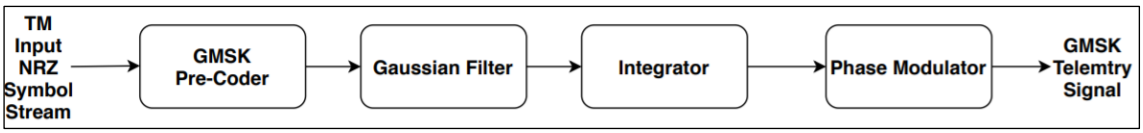

Figure 3-1: GMSK Modulation Schematic [3]

Mathematically, the modulated RF carrier at the output of the phase modulator in Fig. 3-1 is expressed as:

$$x(t) = \sqrt{2Pt}\cos\left[(2\,\pi\,fc\,t + \varphi_{TM}(t-\tau_{TM})\right] \quad (9)$$

Where Pt is the transmitted power, fc the carrier frequency and $\varphi_{TM}(t-\tau_{TM})$ is the phase of the pre-coded GMSK signal which is defined by equations (2), (3) and (4).

Particularizing these equations with a modulation index $h = 0.5$ for a GMSK, it's obtained:

$$\varphi(t,\alpha) = \frac{\pi}{2\cdot Tb}\sum_{n}\alpha_n \int\left\{Q\left(\frac{2\pi BTb}{\sqrt{ln2}} * \left(\frac{\tau}{Tb} - (n+1)\right)\right) - Q\left(\frac{2\pi BTb}{\sqrt{ln2}} * \left(\frac{\tau}{Tb} - n\right)\right)\right\} d\tau \quad (10)$$

Analysing equation (10) and as it has been explained in **2.4.1** (C.P.M Model and GMSK), the pulse which defines the instantaneous frequency of the modulation $g(t)$, is characterized by the parameter BTb, whose values are restricted by the CCSDS to be $0.25\ or\ 0.5$.

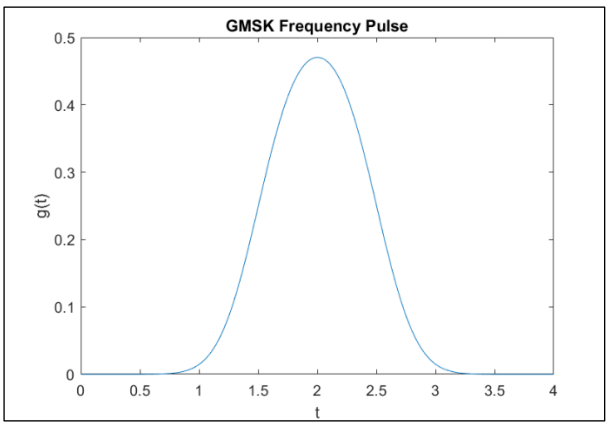

Figure 3-2: g(t) pulse with B·Tb = 0.5

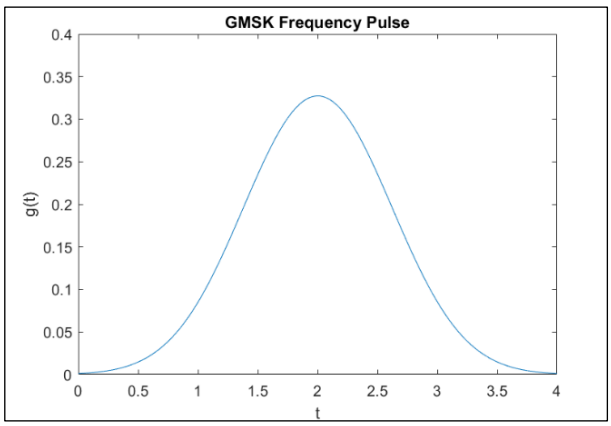

Figure 3-3: g(t) pulse with B·Tb = 0.25

Smaller BTb values result in a wider time domain pulse, introducing more ISI since the pulse spreading over symbols is higher compared to a bigger BTb value, as it can be seen in Fig. 3-3, thus, leading to a higher pulse overlapping in time and a more difficult differentiation between symbols.

Moreover, the resulting spectrum tends to compress as the value is decreased, hence, it appears a trade-off on selecting its value.

Based on that, CCSDS recommends certain values on whether the mission is of category A or B.

According to the standard, a mission is considered of category B if it is located at an altitude greater than $2 \cdot 10^6\ Km$ and $BTb = 0.5$ is selected, otherwise it is an A category mission and $BTb = 0.25$ **[1].**

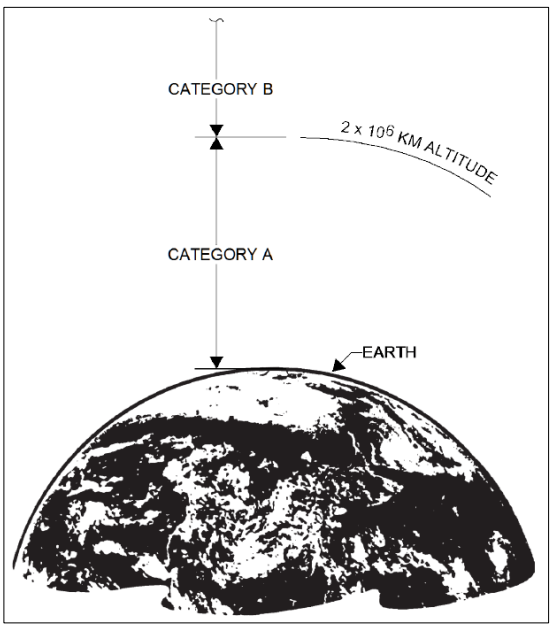

Figure 3-4: Mission Categories

Next, a_k are the pre-coded symbols to be transmitted with $Tb = \frac{1}{Rb}$, obtained from the NRZ bit stream i.e. ± 1 level telemetry (see Fig. 3-6) defined by $a_k = (-1)^{k+1} d_k d_{k-1}$ as shown in Fig 3-5.

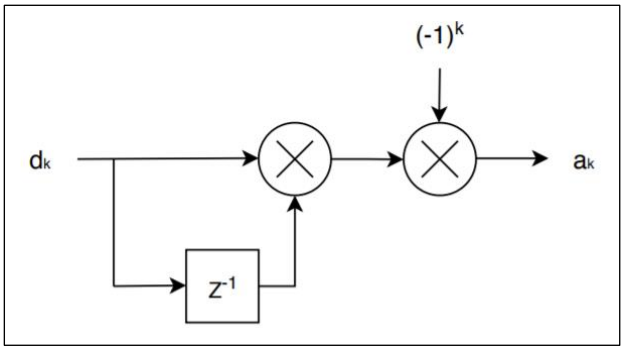

Figure 3-5: GMSK Pre-Coder

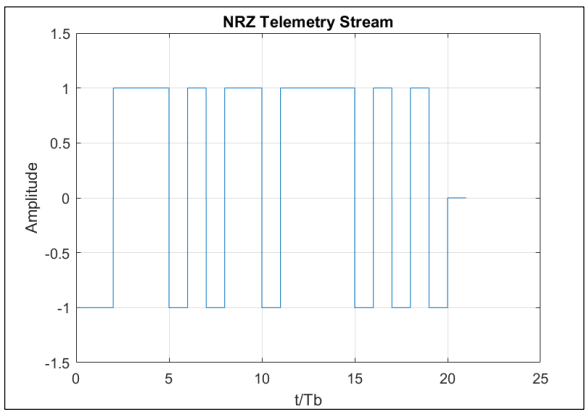

Figure 3-6: Rectangular Pulse Train

Such symbol stream is processed through the Gaussian Filter (see Fig. 3-2 and 3-3) with their respective selected parameter, in order to get the signal shown next, that will be used to generate the phase.

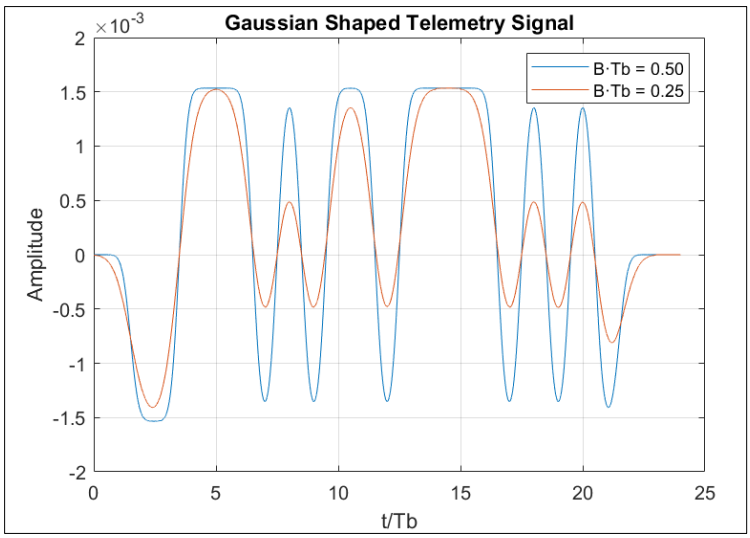

Figure 3-7: TM Frequency Pulse Stream

Once the symbol stream passes through the signal shaping pulse, to meet the constant phase requirement, an integrator is used. In this way, it's obtained at the output of the block the signal that will define the phase evolution during the symbol transmission.

A possible phase signal can be observed in the following Fig. 3-8 and Fig. 3-9 with a BTb equal to 0.25 and 0.50 respectively.

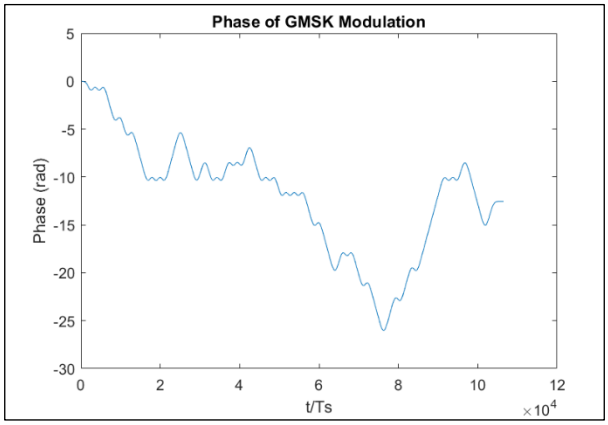

Figure 3-8: Phase Signal with B·Tb = 0.25

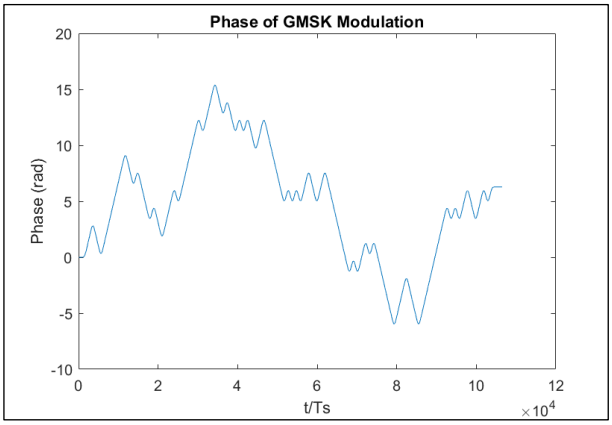

Figure 3-9: Phase Signal with B·Tb = 0.50

Unlike an MSK modulation, here it can be seen the usefulness of the Gaussian filter, since the transitions between the phases are much smoother while with an MSK they would be slightly more abrupt due the use of a rectangular pulse.

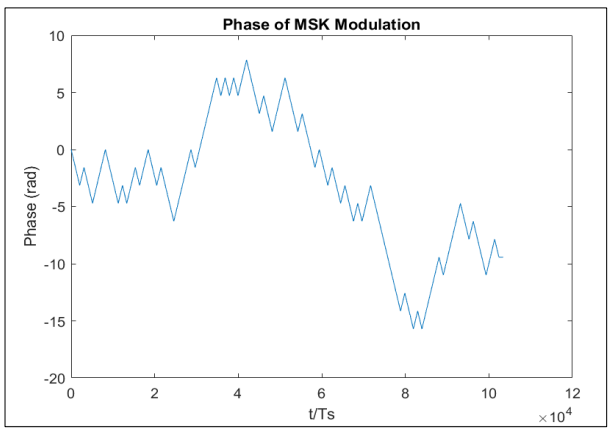

Figure 3-10: MSK Phase Signal

Finally, the signal output of the integrator goes through a phase modulator (PM) which completing a frequency modulator scheme, results in the GMSK modulated signal:

$$b(t)_{TM} = e^{i\varphi(t,\alpha)} \qquad (11)$$

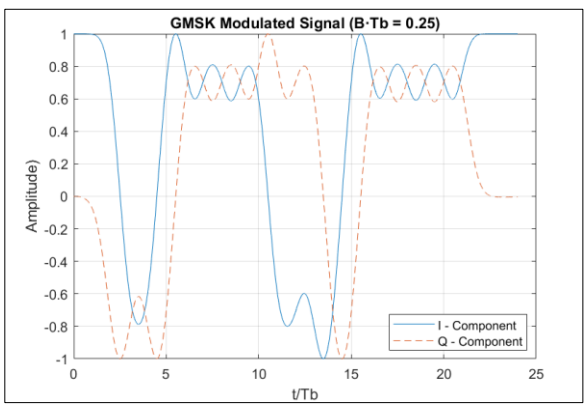

Figure 3-11: I-Q GMSK Modulated Signal (B·Tb = 0.25)

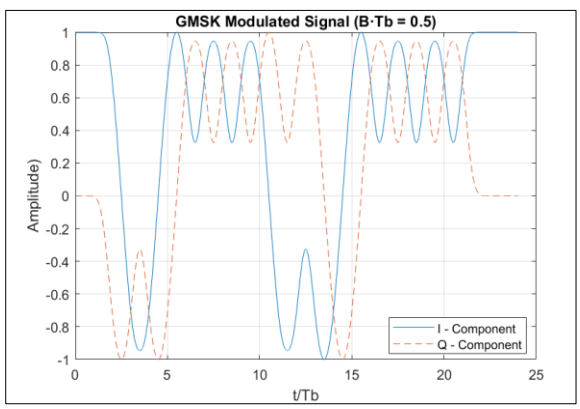

Figure 3-12: I-Q GMSK Modulated Signal (B·Tb = 0.50)

3.1.2. Ranging structure and generation

Regarding the ranging, the following scheme is presented below in Fig. 3-13.

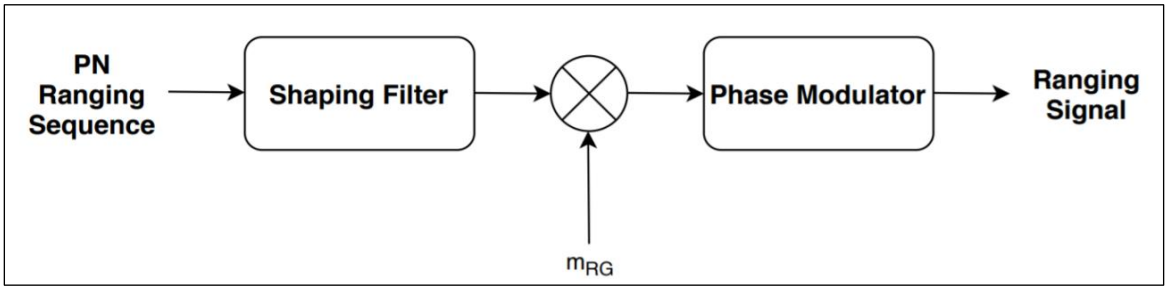

Figure 3-13: Ranging Generation Schematic

The PN Ranging code is linearly modulated on the downlink carrier, i.e. a transition of ± 1 pulses in the baseband code that results into a phase shift of the RF carrier signal obtaining:

$$x(t) = \sqrt{2Pt}\cos\left[(2\,\pi\, fc\, t + \varphi_{RG}(t - \tau_{RG})\right] \quad (12)$$

First, $\varphi_{RG}(t)$ is the ranging phase defined by (13) as:

$$\varphi_{RG}(t) = m_{RG} \cdot \sum_{k} C_k \cdot h(t - kTc) \quad (13)$$

Where m_{RG} is the ranging index, $h(t)$ the impulse response of the shaping filter and C_k are the chip codes (see Table 3) with a chip duration of Tc.

Table 3: Component Codes

C_1	$1, -1$
C_2	$1, 1, 1, -1, -1, 1, -1$
C_3	$1, 1, 1, -1, -1, -1, 1, -1, 1, 1, -1$
C_4	$1, 1, 1, 1, -1, -1, -1, 1, -1, -1, 1, 1, -1, 1, -1$
C_5	$1, 1, 1, 1, -1, 1, -1, 1, -1, -1, -1, -1, 1, 1, -1, 1, 1, -1, -1$
C_6	$1, 1, 1, 1, 1, -1, 1, -1, 1, 1, -1, -1, 1, 1, -1, -1, 1, -1, 1, -1, -1, -1, -1$

Generally, ranging shaping pulses are usually rectangular. Since the beginning, the importance of spectral efficiency has been highlighted, therefore, in order to maximize the use of the spectrum as efficient as possible but keeping it simple and to be able to maintain it at high rates with higher modulation indexes, a sine shaped pulse has been chosen.

As it will be seen in the spectrum verification section, sine choice is justified pulse due its frequency performance. In this way, the impulse response of the filter $h(t)$ is defined as:

$$h(t) = h_{sin}(t) = \begin{cases} \sin\left(\frac{\pi \cdot t}{Tb}\right), & t \in [0, Tc] \\ 0, & elsewhere \end{cases} \quad (14)$$

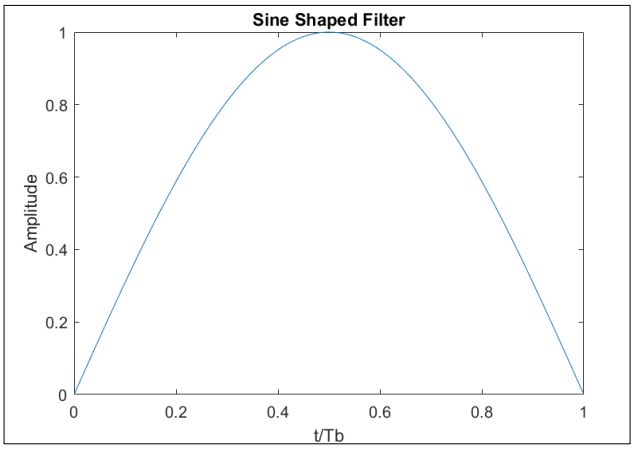

Figure 3-14: Ranging Shaping Filter h(t)

Once the code passes through the shaping pulse and thus the ranging signal is formed, it will be weighted before phase modulation by a ranging index m_{RG} as indicated in Fig. 3-13. Therefore, m_{RG} will define the impact of the ranging with respect to the telemetry, that will be transmitted simultaneously in the complete transmitter.

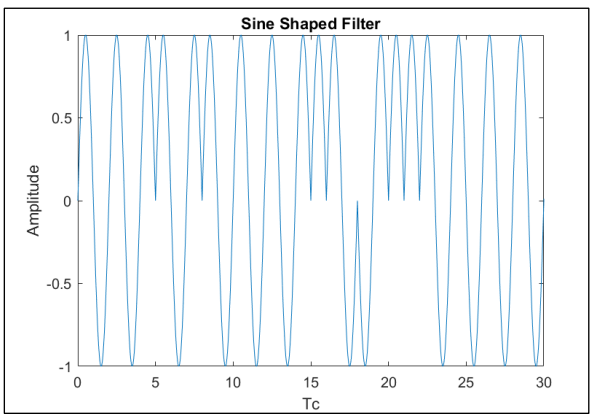

Figure 3-15: T2B Code Sequence

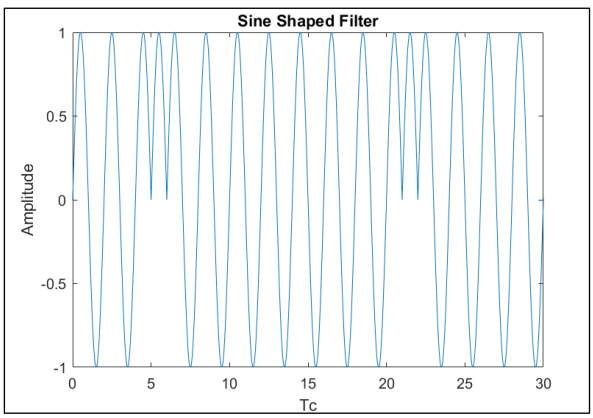

Figure 3-16: T4B Code Sequence

As suggested by equations (5) and (6), the range clock C_1 have a disproportioned influence on the composite code $C_{T2B}\ and\ C_{T4B}$, weighting the signal by a factor 2 and 4 respectively, and therefore the signal's power lies at the range-clock frequency.

Moreover, because of that balance, the composite signal may be viewed as the range clock with an occasional inversion of a chip and consequently its frequency is $fc = \frac{1}{2 \cdot Tc}$.

In Figs. 3.15 and 3.16 it can be seen that the sequence T4B that by granting 4 "votes" to clock-component C_1, the resultant signal tends to the latter.

At last and to end with the ranging block, the ranging sequence is phase modulated as it was done with the telemetry signal obtaining the following signal:

$$b_{RG} = e^{i \cdot \varphi_{RG}(t)} \tag{15}$$

3.1.3. Simultaneous Transmission of Telemetry and Ranging

Once the transmitters of both signals with their respective characteristics and operation have been shown, the complete simultaneous transmission scheme recommended by the CCSDS standard is presented in the following Fig. 3-17.

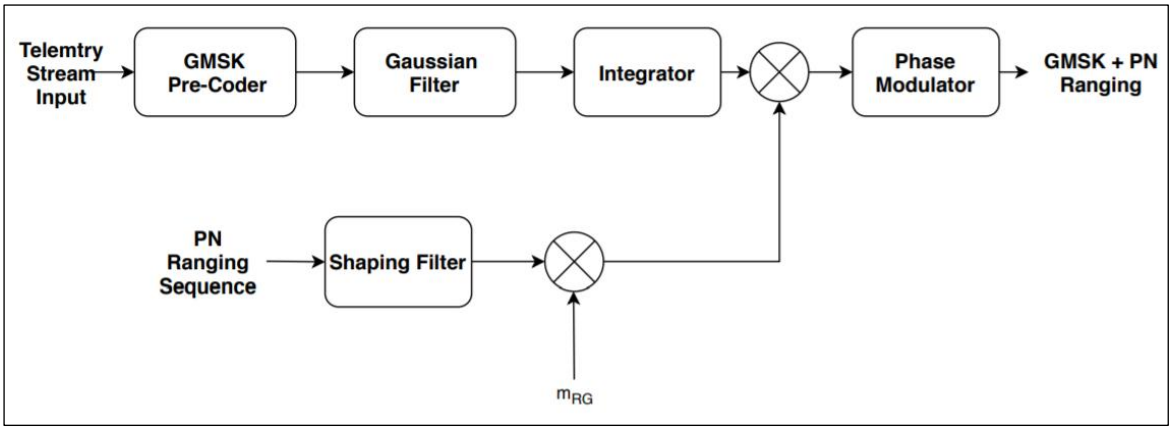

Figure 3-17: GMSK + PN Ranging Schematic [3]

Analogously to the presented transmitters and as the scheme suggests, the signal at the output of the phase modulator i.e. the lowpass equivalent is defined by (16):

$$b_x(t) = e^{i\cdot\varphi_{TM}(t-\tau_{TM})}e^{i\cdot\varphi_{RG}(t-\tau_{RG})} \tag{16}$$

Where $\varphi_{TM}(t-\tau_{TM})\ and\ \varphi_{RG}(t-\tau_{RG})$ are the telemetry and ranging modulated phase shifts withing the compete modulated RF signal to be transmitted in the downlink.

$$x(t) = \sqrt{2Pt}\cos\left[(2\,\pi\,fc\,t + \varphi_{TM}(t-\tau_{TM}) + \varphi_{RG}(t-\tau_{RG})\right] \tag{17}$$

3.1.4. Signal Model Validation

Once our transmission system has been implemented and its temporal behaviour analysed, it is necessary to study the set of signals in the frequency domain, since it is where the requirements established in the project, among many, spectral efficiency must be satisfied.

3.1.4.1. Telemetry in Frequency Domain

First of all, and as an imposition by the standard, the telemetry signal has to be compliant with the spectral mask mentioned in section **2.3.** (CCSDS Standard and SFCG Mask).

Next Figs. 3-18, 3-19, 3-20 and 3-21 show both GMSK telemetry PSD with their respective $B \cdot Tb$ value. In addition, two SFCG recommended frequency masks are plotted.

As it can be seen, each mask is related to telemetry rates under and above $2\ Ms/s$ which is a boundary for the definition of high symbol rates adopted by CCSDS. Depending on which rate is selected for the mission, the spectrum has to fall under the associated mask to meet a bandwidth limit.

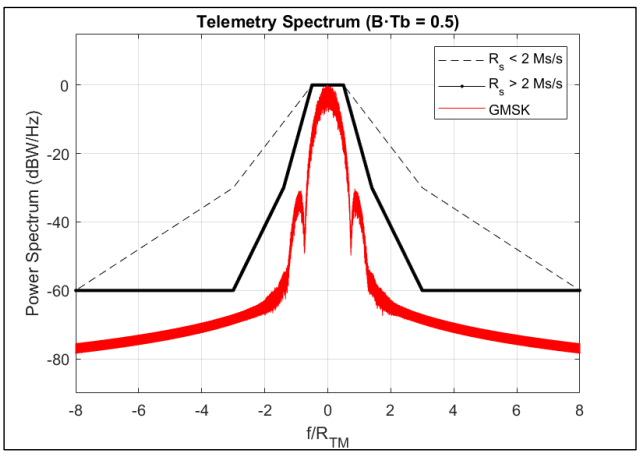

Figure 3-18: Telemetry Spectrum B·Tb = 0.50

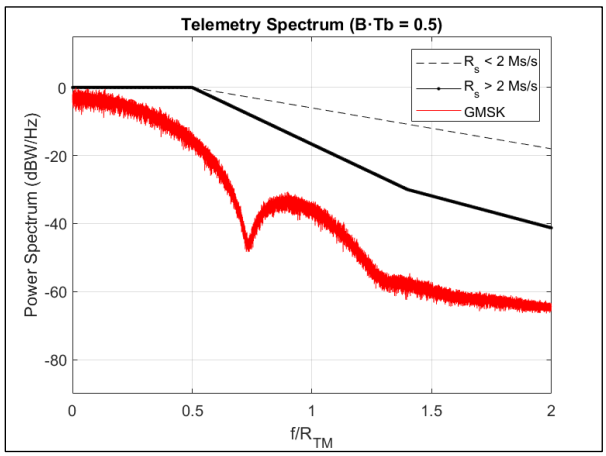

Figure 3-19: Telemetry One-Sided Spectrum

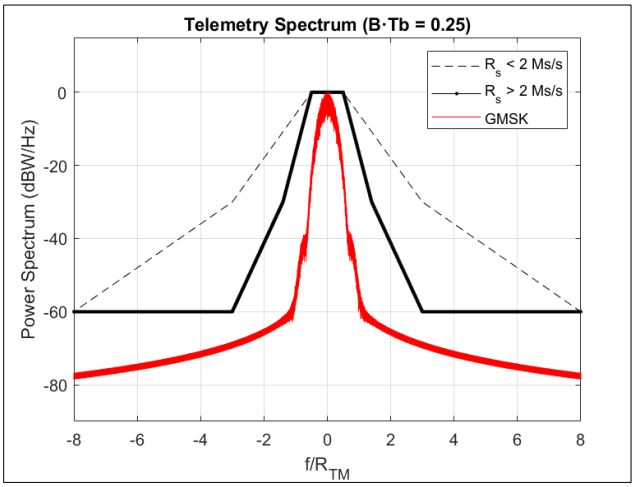

Figure 3-20: Telemetry Spectrum B·Tb = 0.25

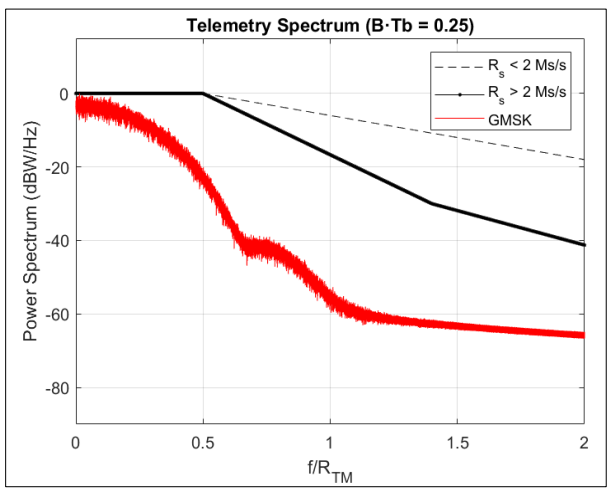

Figure 13: Telemetry One-Sided Spectrum

For both, $B \cdot Tb$ = 0.5 and $B \cdot Tb$ = 0.25 the spectrum related only to telemetry is compliant with mask recommendation.

Furthermore, as $B \cdot Tb$ decreases, the secondary lobes also decrease as represented in the close-up figures, leading to a more closed and spectrally efficient spectrum but as it's explained in **3.1.1** (Telemetry structure and generation) it impacts negatively increasing ISI.

3.1.4.2. Ranging in Frequency Domain

On the other hand, ranging spectrum basically depends on the shaping filter used and the type of code selected among T_2B and T_4B. In order to justify the sine shaping filter used it's interesting to study its behaviour while transmitting both telemetry and ranging simultaneously.

Next, Figs. 3-22, 3-23, 3.24 and 3.25 show both ranging sequences spectra:

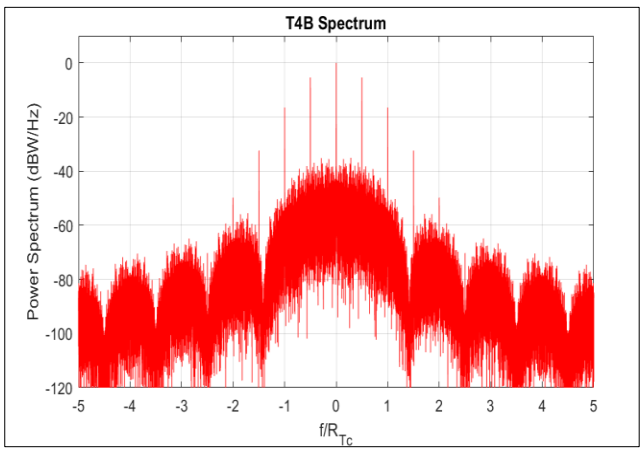

Figure 3-22: T4B Spectrum

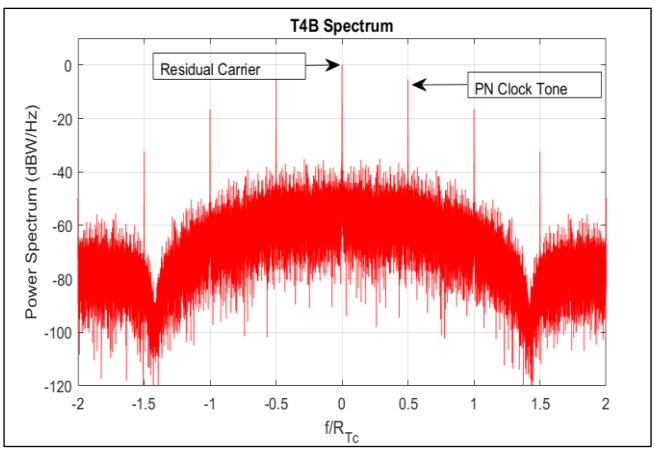

Figure 3-23: T4B Spectrum Close-Up

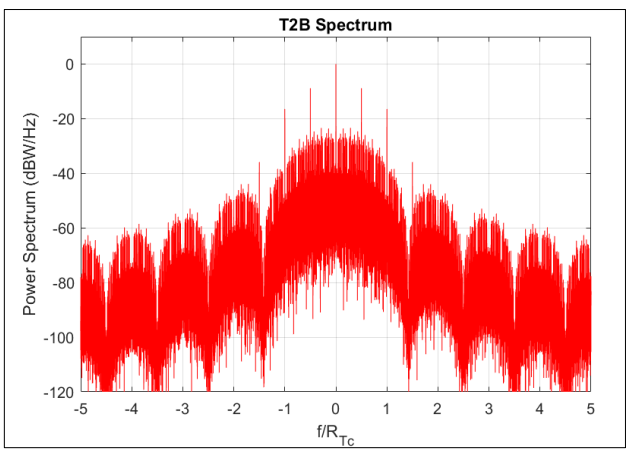

Figure 3-24: T2B Spectrum

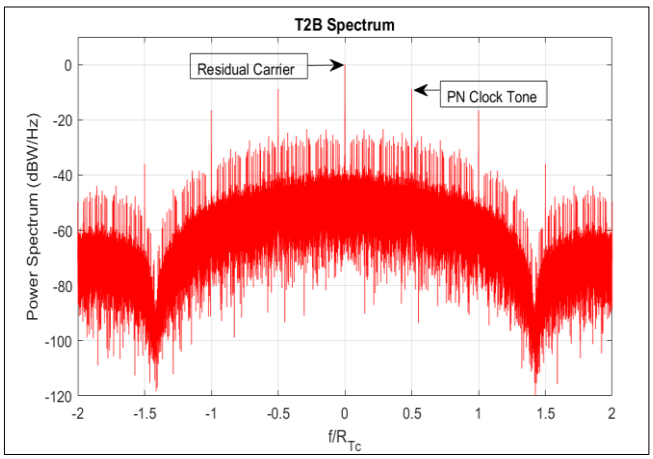

Figure 3-25: T2B Spectrum Close-Up

In **3.1.2** (Ranging structure and generation) it is highlighted the fact that both codes have a disproportionated sequence C_1 respect other components. This is also reflected on the plots, since a strong clock component is found at a one half the chip rate as it's indicated, in accordance with the frequency of the main component of the code.

Comparing the current filter with a possible alternative as could be a rectangular pulse shown in Fig. 3-26 below, how sine shaped filter also decays in frequency relatively in comparison with squarewave shaping.

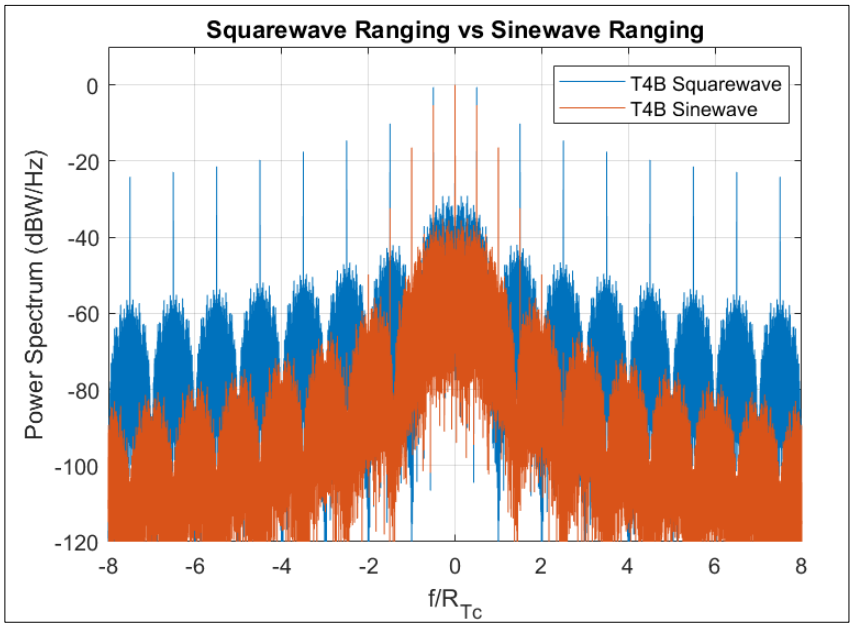

Figure 3-26: Sinewave vs. Squarewave Ranging

3.1.4.3. Simultaneous Transmission frequency validation:

Once studied the spectral characteristics of both signals separately, it is time to study the behaviour of the combination of both and what are the effects of ranging on the telemetry signal.

The standard imposes for the simultaneous transmission of ranging a chip rate to telemetry rate greater than one, limiting to the range from **1** to **3**.

Basically, in this section will be studied the lower bound rate ratio $\frac{R_{RG}}{R_{TM}} \geq 1$ and the upper bound rate ratio $\frac{R_{RG}}{R_{TM}} \geq 3$ **[3].**

The following simulations allow a general study of the effects of choosing the PN codes $T2B$ and $T4B$, the impact of an unbalance between the ranging and telemetry rate ratios as well as the impact of increasing the ranging modulation index.

These simulations take into account the next characterized parameters:

- m_{RG} values chosen in a range of **[0.111, 0.222, 0.444, 0.666].**
- $\frac{R_{RG}}{R_{TM}} \geq 1$ and $\frac{R_{RG}}{R_{TM}} \geq 3$.
- Sinewave $T2B$ *and* $T4B$ ranging sequences.

Impact of Ranging on the GMSK:

Figs. 3-27, 3-28, 3-29 and 3-30 show for a ranging-telemetry ratio equal to one, the spectrum of a combined GMSK plus sinewave shaped Ranging for different $B \cdot Tb$ values and code types.

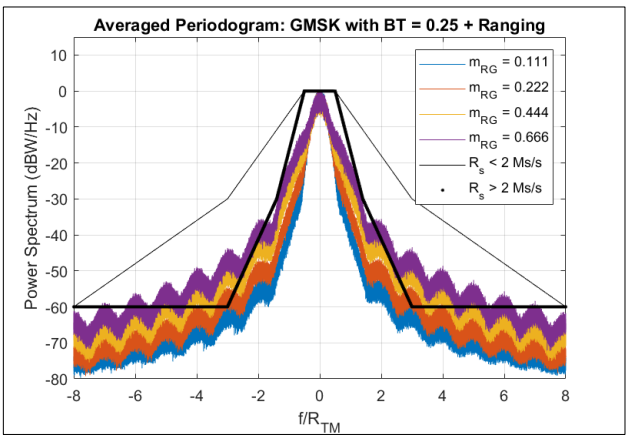

Figure 3-27: GMSK (B·Tb = 0.25)/PN(Sine) Spectral Plots for T2B Code

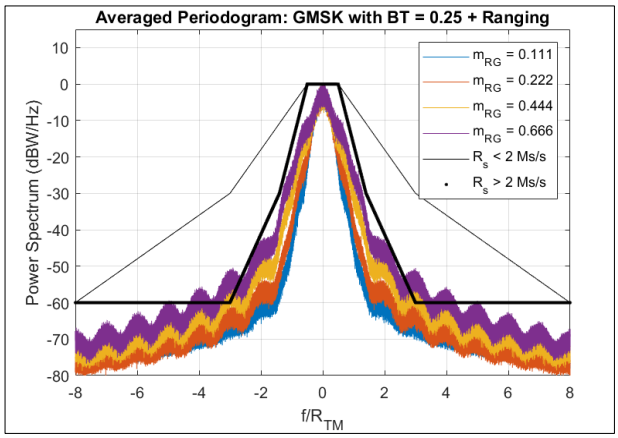

Figure 3-28: GMSK (B·Tb = 0.25)/PN(Sine) Spectral Plots for T4B Code

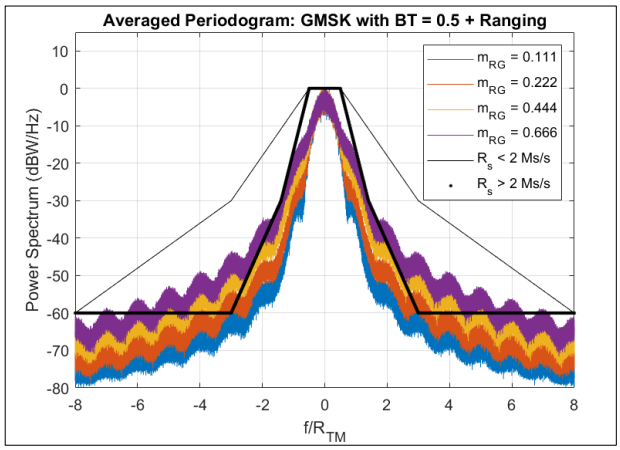

Figure 3-29: GMSK (B·Tb = 0.50)/PN(Sine) Spectral Plots for T2B Code

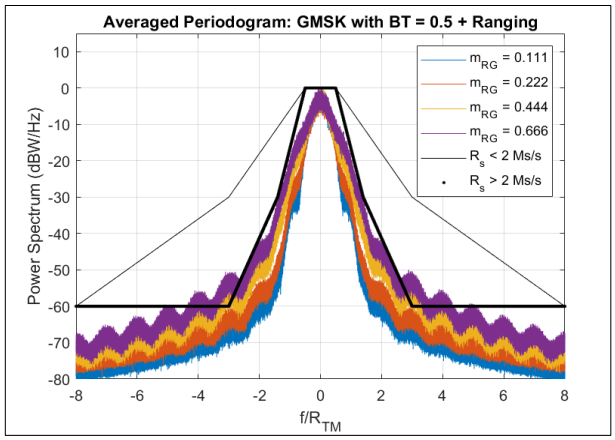

Figure 3-30: GMSK (B·Tb = 0.50)/PN(Sine) Spectral Plots for T4B Code

As mentioned in section **2.3** (CCSDS Standard and SFCG spectral Mask), the spectral mask does not apply to the ranging but only to telemetry. Although, it's used to provide an indication of how good the selected simultaneous telemetry and ranging transmission can be from a spectral management point of view.

In preview and as can be deduced by (13), the impact of the range on the telemetry signal is proportional to the modulation index. The larger the selected value, the more prominent the spectral features of the ranging signal (secondary lobes) and the GMSK undergoes a clear distortion followed by a widening of the spectrum.

An interesting parameter to compute and see ranging impact, is the normalized occupied bandwidth, which shows the amount of bandwidth that concentrates about the 99% of the transmitted power.

As it can be seen in Table 4, when ranging is combined with Telemetry, selecting $T4B$ has a narrower bandwidth than $T2B$ when a large ranging index (0.444 or 0.666) is selected, thus, performing better as it can be seen in Figs. 3-27, 3-28, 3-29 and 3-30.

Table 4: Normalized Occupied Bandwidth

	$\mathbf{B \cdot Tb = 0.5}$		$\mathbf{B \cdot Tb = 0.25}$	
Ranging Index	**T2B**	**T4B**	**T2B**	**T4B**
0.111	1.059	1.065	0.890	0.901
0.222	1.175	1.203	1.050	1.095
0.444	1.679	1.610	1.550	1.470
0.666	1.991	1.861	1.901	1.710

Furthermore, $T2B$ is slightly less bandwidth efficient and under the same conditions exceeds the mask, e.g., for a ranging index of 0.222, $T4B$ falls under the mask and the

opposite occurs with $T2B$ for both bandwidth-time products. This can be seen also in Figs. 3-27, 3-28, 3-29 and 3-30.

Thus, both codes comply with the mask by establishing a boundary in terms of the range index.

No less important, to see the impact of the choice of a sinewave instead of the squarewave, in the following Figs. 3-31 and 3-32, the telemetry spectrum squarewave ranging can be seen.

In both figures, in the most favourable case for both TM modulations, which is selecting the T4B code, the mask is completely exceeded. In addition, there's no roll-off appreciable even for low ranging indexes. For this reason, it is completely discarded since it has no advantages respect sinewave.

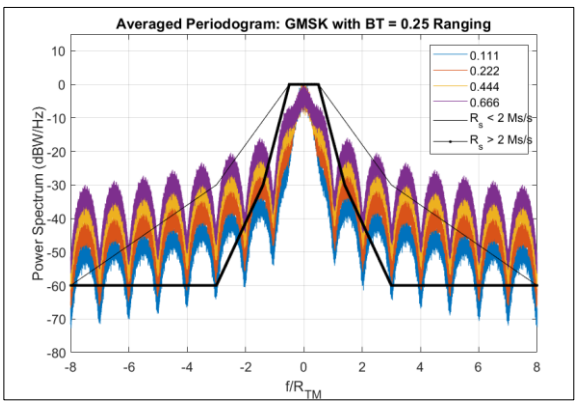

Figure 3-31: GMSK (B·Tb = 0.25)/PN(Squarewave) T4B Spectrum

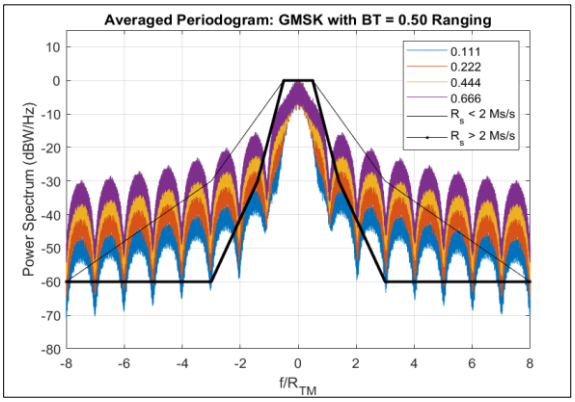

Figure 3-32: GMSK (B·Tb = 0.50)/PN(Squarewave) T4B Spectrum

Lastly, it is important to analyse the case in which there is an imbalance in the ratio of the range rate to the telemetry.

So, next case focuses on a chip ranging to telemetry ratio ($\frac{R_{RG}}{R_{TM}}$) greater than 1 and as defined by the standard, limited to 3.

As will be seen in this case, the spectrum becomes much more abrupt, exceeding the spectral mask as illustrated in Figs. 3-33, 3-34, 3-35 and 3-36.

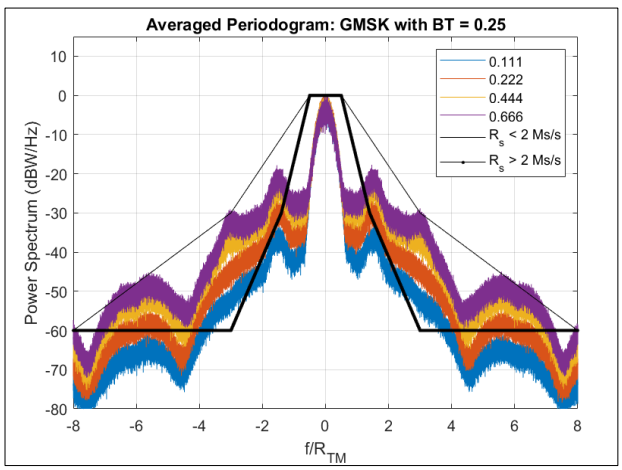

Figure 3-33: GMSK (B·Tb = 0.25)/PN(Square) T2B with rate ratio 3

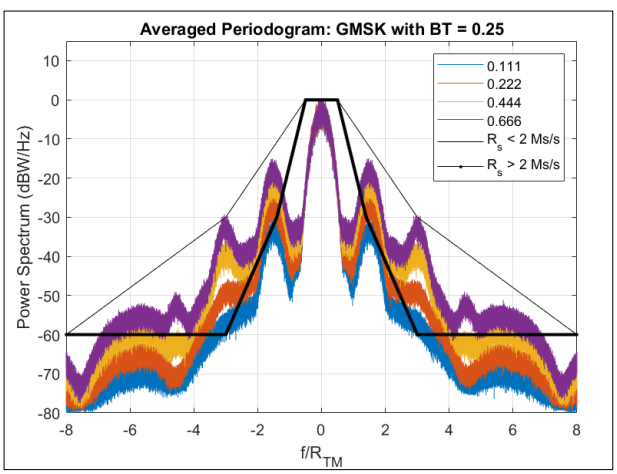

Figure 3-34: GMSK (B·Tb = 0.25)/PN(Square) T4B with rate ratio 3

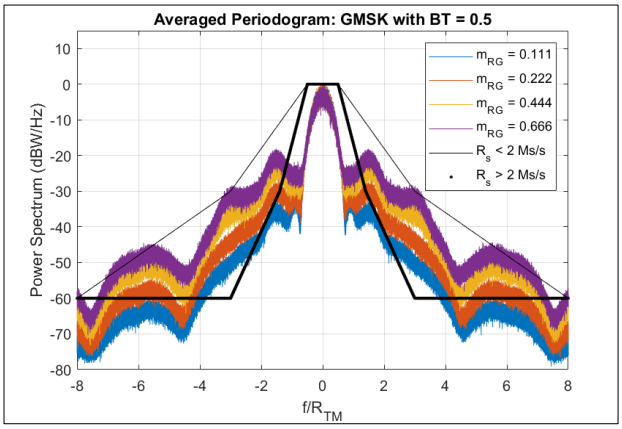

Figure 3-35: GMSK (B·Tb = 0.50)/PN(Square) T2B with rate ratio 3

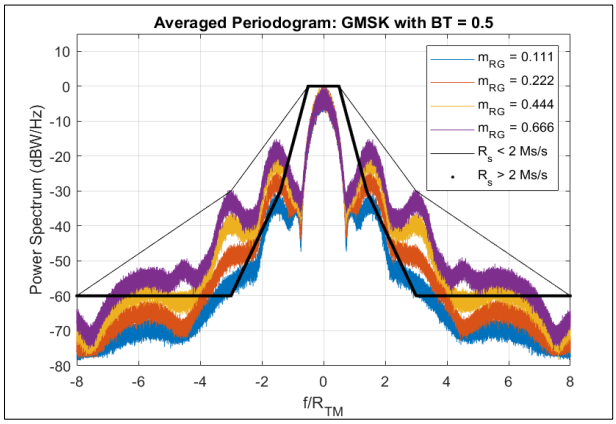

Figure 3-36: GMSK (B·Tb = 0.50)/PN(Square) T4B with rate ratio 3

Unlike what happened in the previous case, for $\frac{R_{RG}}{R_{TM}}$ > **3**, the spectrum does not fit under the mask in a clearer way, reaching the border of the mask destined for rates below 2 Ms/s. Even selecting beneficial parameters, such as a small ranging value of 0.222, code T4B can lead to a slightly narrower band but even for $B \cdot Tb$ of 0.25 it's not possible to fall under the boundary, hence the spectral behaviour is worse due the higher rate unbalance.

3.2. Receiver

Once raised the operation and design of the transmitter that will be part of our downlink focused communication system, based on standard's recommendations, we will present the design of our reception system.

As we discussed in the transmitter chapter, the standard CCSDS is much more flexible in terms of receiver design allowing us to explore different options and techniques according to mission requirements.

In this case, the standard presents a high-level scheme of the transmitter, emphasizing the main characteristics that it must have shown in the next Fig. 3-37:

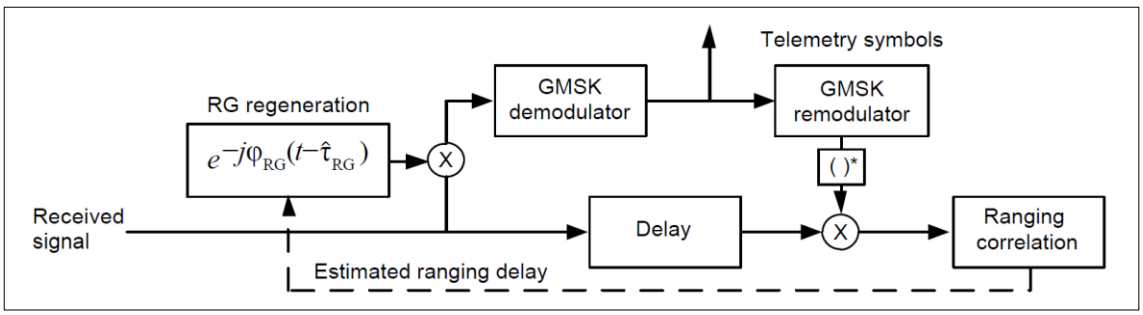

Figure 3-37: High-Level Diagram of GMSK + PN Ranging ***[1]***

One of the requirements and standard recommendation is Ranging Cancellation which should be applied to the receiver.

In addition, the standard also proposes a possible design, in this case, already specifying the blocks that make up the GMSK demodulator and techniques that will be used for the detection of telemetry shown next:

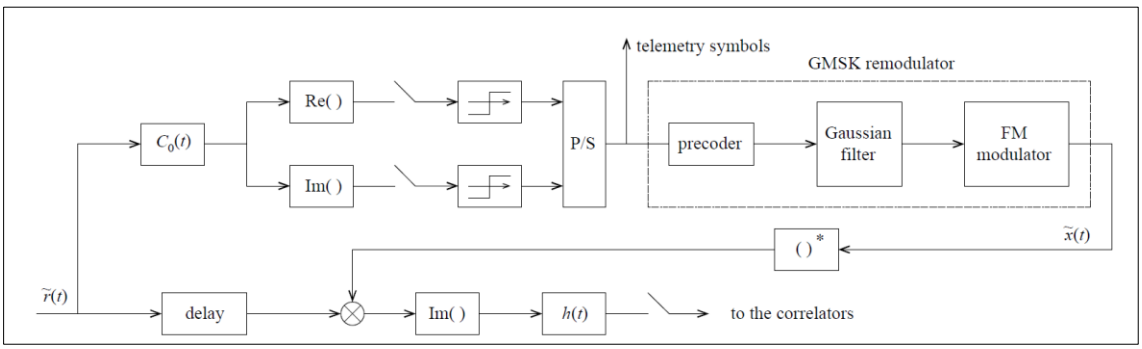

Figure 3-38: Possible Demodulator Schematic for GMSK + PN Ranging ***[1]***

As reflected in the scheme, this receiver is based on the Laurent decomposition ($Co(t)$ filter) with $B \cdot Tb$ = 0.5 and an additional Wiener filter in case a $B \cdot Tb$ = 0.25 is used due the ISI increment.

Likewise, the receiver that will be raised next, named Kaleh **[7][8]** receiver, is also based on the Laurent Decomposition which will allow us to propose a low complexity demodulator, much more versatile, that will serve for both values of the GMSK without changing any feature.

3.2.1. Telemetry Receiver

3.2.1.1. Laurent Expansion

One of the most interesting CPM's representations is the so-called Laurent Expansion, a representation defined by the homonymous author, more than a decade ago.

Laurent Expansion represents a CPM modulation in the form of a superposition of phase-shifted amplitude-modulation pulse (AMP) streams, the number of such being dependent on the amount of partial response in the modulation **[9][7].**

GMSK is a modulation with memory and unlike the MSK that is full-response and memoryless, a single pulse will not be enough to define it.

Through analysis and mathematical development of the complex baseband telemetry signal (11), the following expression is reached **[7]:**

$$\boldsymbol{S(t) = \sqrt{2 \cdot Pt} \sum_{K=0}^{2^{L-1}-1} \left[\sum_{n=-\infty}^{\infty} e^{i \cdot \frac{\pi}{2} A_{k,n}} \cdot C_k(t - nTb) \right]}$$
$$\boldsymbol{\triangleq \sqrt{2 \cdot Pt} \sum_{K=0}^{2^{L-1}-1} \left[\sum_{n=-\infty}^{\infty} \tilde{a}_{K,n} \cdot C_k(t - nTb) \right]} \quad (18)$$

Resulting in an expression in the form of pseudo-symbols and a stream of pulses that as we will see below will have different durations and therefore the overlapping between these is demonstrated.

Since the frequency pulse structure $g(t)$ is dependent on the Q function, which is infinite in its extent, it is common to truncate the pulse so as to deal with a finite ISI.

Hence, it forces to introduce a parameter L, which appears in the equation above. It's a parameter that serves to define the duration of the frequency pulse, i.e., since the GMSK is a partial response modulation, the duration of the pulse is greater than that of a bit time $L \cdot Tb$. The value of L will vary depending on $B \cdot Tb$, that is, coherent with the spread of the pulse in time, and thus taking into account a correct amount of ISI.

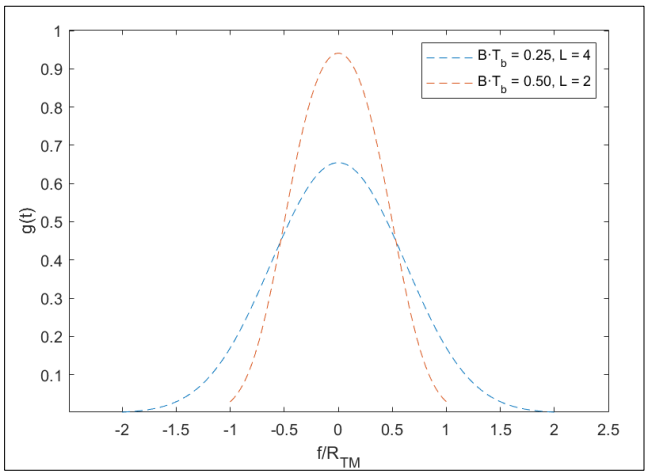

Figure 3-39: Truncated Frequency Pulse

Starting from equation (18), it shows that the signal is formed by 2^{L-1} amplitude pulse trains on which each $C_k(t)$ is the equivalent pulse shape for the k_{th} transmission that can be determined by the function defined by:

$$\boldsymbol{\Psi(t)} = \begin{cases} \boldsymbol{\pi \cdot q(t)}, & \boldsymbol{0 \le t \le L \cdot Tb} \\ \boldsymbol{\frac{\pi}{2}[1 - 2q(t - L \cdot Tb)]}, & \boldsymbol{L \cdot Tb \le t} \end{cases} \qquad \textbf{(19)}$$

Psi function ($\boldsymbol{\Psi(t)}$) is basically obtained by reflecting the nonconstant part of the phase pulse *q*(*t*) (3), that exists in the interval $0 \le t \le LTb$ about the $t = L \cdot Tb$ axis as it is shown in Figs. 3-40 and 3-41.

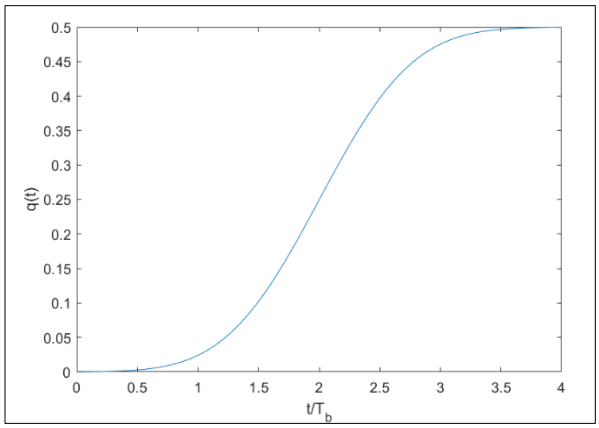

Figure 3-40: q(t) function for B·Tb = 0.25, L=4

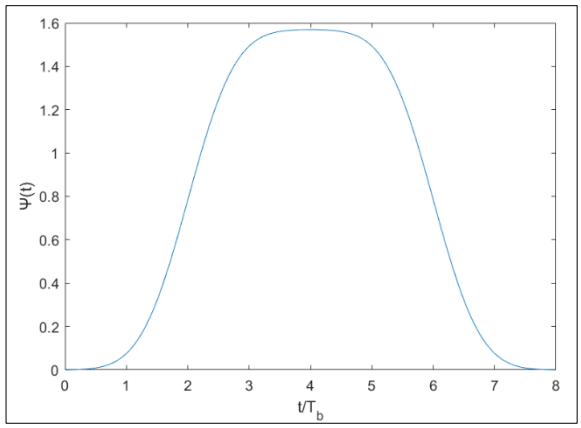

Figure 3-41: Ψ(t) function for B·Tb = 0.25, L=4

Therefore, in view of, $\Psi(t)$ is a waveform that is nonzero in the interval $0 \le t \le 2LTb$ and symmetric around $t = LTb$.

Once the previous function is obtained, we arrive at the definition of $S_n(t)$, which is nothing more than the sine applied to the Psi function and then shifted a number of times the duration of a bit:

$$S_n(t) \triangleq S_o(t + nT) = sin\big(\Psi(t + nT)\big) \qquad (20)$$

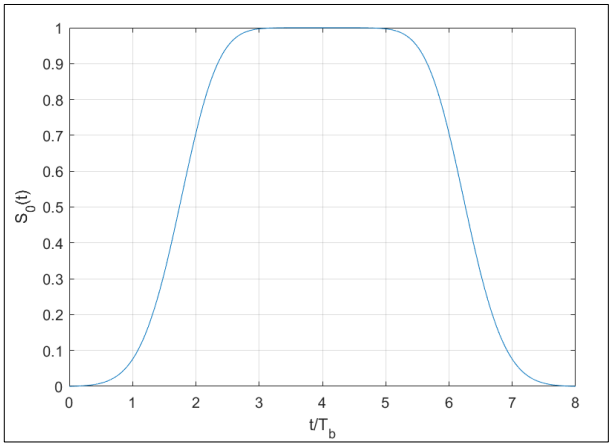

Figure 3-42: So(t) function

Finally, we come to the definition of $C_k(t)$:

$$C_k(t) = S_o(t)\prod_{i=1}^{L-1} S_{i+L\beta_{k,i}(t)}, \qquad 0\leq K\leq 2^{L-1}-1, \quad 0\leq t\leq T_{bK} \tag{21}$$

$$T_{bK} = T_b x \min_{i=1,2,\ldots,L-1}\left[L(2-\beta_{K,i})-i\right] \tag{22}$$

Where $\beta_{K,i}$ are the coefficients that represent the integer K binarily as:

$$K = \sum_{i=1}^{L-1} 2^{i-1}\beta_{K,i} \tag{23}$$

From (22) it can be appreciated that every pulse has a different duration T_{bK} and so (18) is a pulse stream which consists on overlapping pulses.

As a last factor to analyse and not less important, which will be key to understand the demodulator approach, is the complex phase (pseudo-symbols) defined also in (18).

In particular each phase is associated with its respective translated pulse $C_k(t-nT)$ and can be expressed in function of $\beta_{K,i}$, i.e. the binary representation of K as follows **[7]:**

$$A_{k,n} = \sum_{i=-\infty}^{n} a_i - \sum_{i=1}^{L-1} a_{n-i}\beta_{K,i} = A_{0,n-i} - \sum_{i=1}^{L-1} a_{n-i}\beta_{K,i} \tag{24}$$

And thus,

$$\tilde{\boldsymbol{a}}_{\boldsymbol{K,n}} \triangleq e^{j\frac{\pi}{2}A_{k,n}} = exp\left[j\frac{\pi}{2}\left(A_{0,n-L} + \sum_{i=-\infty}^{n} a_{n-i} - \sum_{i=1}^{L-1} a_{n-i}\beta_{K,i}\right)\right] \tag{25}$$

$$= \tilde{\boldsymbol{a}}_{\boldsymbol{0,n-L}}\boldsymbol{e^{j\frac{\pi}{2}a_n}}\cdot\prod_{i=1}^{L-1} e^{i\frac{\boldsymbol{\pi}}{\boldsymbol{2}}a_{n-i}\left[1-\beta_{K,i}\right]} \tag{26}$$

Particularizing the equations to our case, the Laurent pulses that will be used to represent our telemetry signal for the two values of $B \cdot Tb$ are presented.

Considering a $B \cdot Tb = 0.25$, to have an adequate representation of a respective the GMSK, a suitable value of $L = 4$ is chosen.

Therefore, from (18) there're $\mathbf{2^{L-1}}$ **,** or what is the same, 8 different Laurent pulses $C_k(t)$ to decompose the modulation.

As described in (21), each $C_k(t)$ is a product of $L = 4$ base generalized pulses $S_n(t)$ chosen accordingly to their index K.

For example, in that particular case and we have $K = 1$:

$$K = 1 = 2^0 \cdot 1 + 2^1 \cdot 0 + 2^2 \cdot 0 \rightarrow \beta_{1,1} = 1, \beta_{1,2} = 0, \beta_{1,3} = 0$$

And thus,

$$C_1(t) = S_o(t) \prod_{i=1}^{L-1} S_{i+L\beta_{1,i}(t)} = S_0(t)S_2(t)S_3(t)S_5(t), \qquad 0 \leq t \leq 3Tb$$

Next Fig. 3-43 illustrates the resulting C_1 Laurent Pulse.

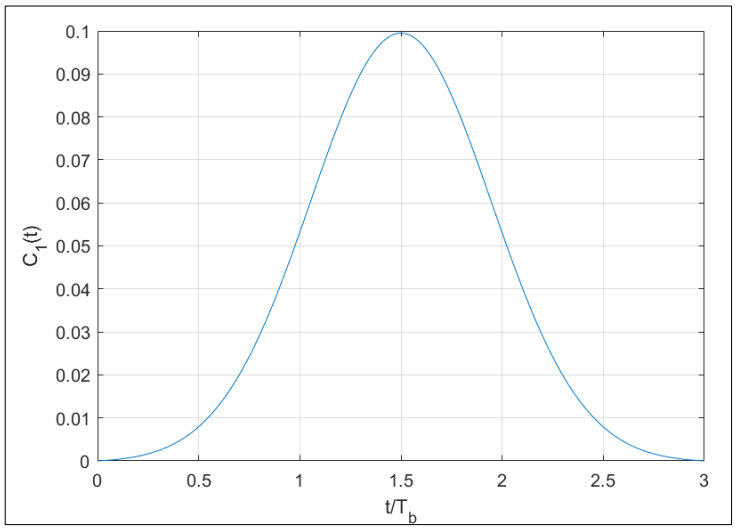

Figure 3-43: C1 Laurent Pulse for L = 4

For each one of the other pulses results in the next combinations grouped on the table 5.

Table 5: Ck Laurent Pulses for L = 4

$C_0(t) = S_0(t)S_1(t)S_2(t)S_3(t)$	$0 \leq t \leq 5Tb$
$C_1(t) = S_0(t)S_2(t)S_3(t)S_5(t)$	$0 \leq t \leq 3Tb$
$C_2(t) = S_0(t)S_1(t)S_3(t)S_6(t)$	$0 \leq t \leq 2Tb$
$C_3(t) = S_0(t)S_3(t)S_5(t)S_6(t)$	$0 \leq t \leq 2Tb$
$C_4(t) = S_0(t)S_1(t)S_2(t)S_7(t)$	$0 \leq t \leq Tb$
$C_5(t) = S_0(t)S_2(t)S_5(t)S_7(t)$	$0 \leq t \leq Tb$
$C_6(t) = S_0(t)S_1(t)S_6(t)S_7(t)$	$0 \leq t \leq Tb$
$C_7(t) = S_0(t)S_5(t)S_6(t)S_7(t)$	$0 \leq t \leq Tb$

From (25) and (26), the complex phase coefficients for the first pulse train corresponding to $C_1(t)$ are:

$$\tilde{\boldsymbol{a}}_{\boldsymbol{1,n}} = \tilde{\boldsymbol{a}}_{\boldsymbol{1,n-4}} \boldsymbol{e}^{\boldsymbol{j\frac{\pi}{2}a_n}} \cdot \prod_{i=1}^{3} e^{i\frac{\pi}{2}a_{n-i}[1-\beta_{0,i}]} = \tilde{\boldsymbol{a}}_{\boldsymbol{1,n-4}} \boldsymbol{e}^{\boldsymbol{j\frac{\pi}{2}a_n}} \cdot \boldsymbol{e}^{\boldsymbol{j\frac{\pi}{2}a_{n-2}}} \cdot \boldsymbol{e}^{\boldsymbol{j\frac{\pi}{2}a_{n-3}}} \quad (27)$$

Analogously, all other $\tilde{a}_{K,n}$ can be calculated.

According to reference **[7],** through computer simulations it is demonstrated that with an $L = 4$, the first pulse C_0, and therefore, the first component of the AMP, contains more than $99{,}194\%$ of the total energy of the signal and the previously developed component C_1 $0{,}803\%$. Therefore, the remaining 7 components have an very low energy-wise impact, a fact that allows us to approximate our TM signal with only 2 stream pulses and grouping more than 99.99% of the total energy of the signal.

In summary, for values of $B \cdot Tb$ in which $L = 4$ is an adequate value, our signal will be approximated exactly by 2 pulses associated to $K = 0$ and $K = 1$ in the form:

$$\tilde{S}_{GMSK}(t) = \sqrt{2Pt}\left[\sum_{i=-\infty}^{\infty} \tilde{a}_{0,n} \cdot C_0(t - nTb) - \sum_{i=1}^{L-1} \tilde{a}_{1,n} \cdot C_0(t - nTb)\right] \quad (28)$$

Where C_0 and C_1 are determined through (21), and likewise, $\tilde{\boldsymbol{a}}_{\boldsymbol{0,n}}$ *and* $\tilde{\boldsymbol{a}}_{\boldsymbol{1,n}}$ from the equations (25) and (26)

Next Fig. 3-44 show Laurent overlapped pulses (C_0, C_1) in time for a $B \cdot Tb = 0.25$.

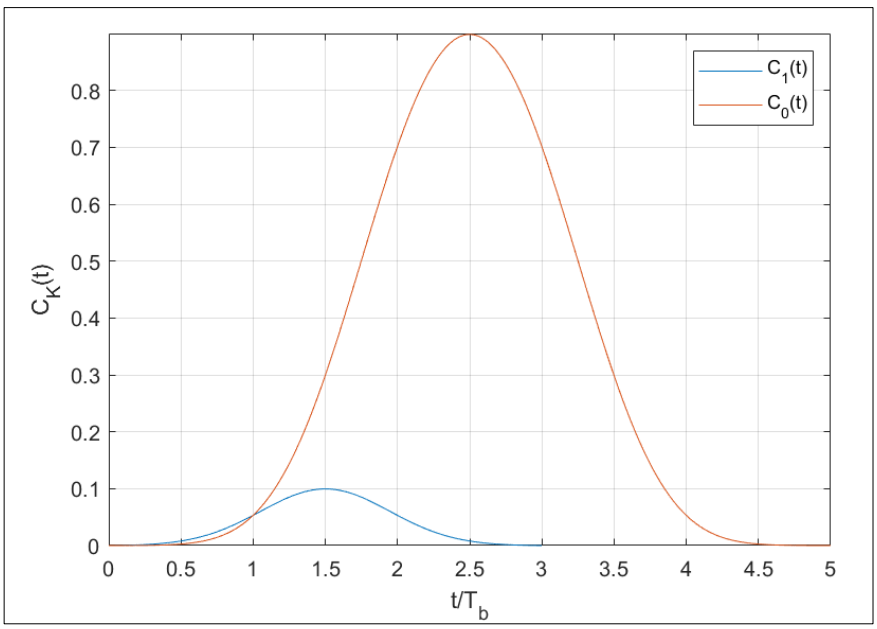

Figure 3-44: Laurent Pulses for K = 0, K=1

3.2.1.2. Coherent Detection: Viterbi Algorithm

There is a wide variety of receptors designed for the consistent detection of GMSK. The vast majority are based on Laurent decomposition and use the Viterbi Algorithm.

As emphasized throughout the document, the GMSK modulation has memory and therefore from the point of view of error minimization, the optimal receiver has an MLSE structure that is generally achieved by the Viterbi Algorithm. In addition, our receiver has no only to work against signal's ISI but to overcome a white noise channel.

This optimal receiver uses $2^{L-1} - 1$ filters, a number that depending on the characteristics of the signal can become relatively high. Each of these filters matches each pulse used in the Laurent decomposition.

Basically, the outputs of the matched filters go as an input to the VA whose metrics which will be soon explained, will be in charge of selecting the transmitted sequence.

Such receiver has the next structure shown below in Fig. 3-45.

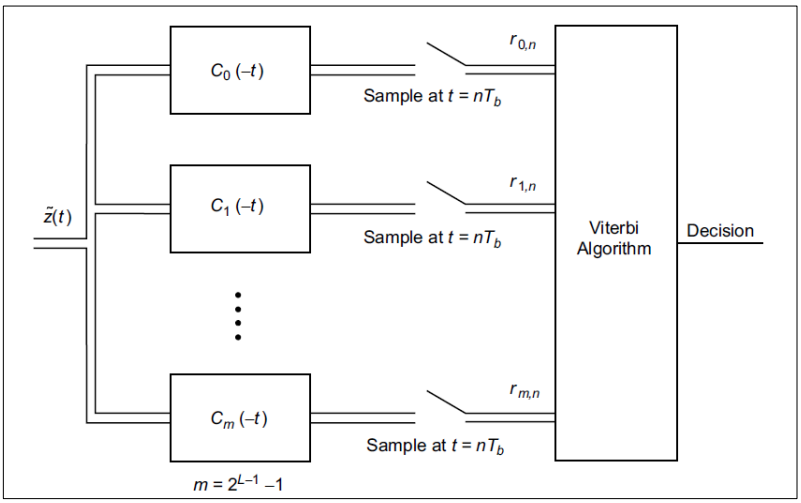

Figure 3-45: Optimum GMSK Receiver [7]

Let's begin defining the transmitted signal which is composed by the modulated telemetry and a white noise component acquired through downlink transmission:

$$z(t) = s(t) + n(t) \tag{29}$$

Then for an N length sequence, all of the possible 2^N transmitted signals have equal energy and are equally likely, the optimum receiver presented above minimizes error through selecting only the ith sequence that maximize the following metric:

$$\Lambda_i = 2 \cdot \int_{-\infty}^{\infty} z(t) \cdot s_i(t)\, dt = Re\left[\tilde{Z}(t) \cdot \tilde{S}_i(t)^*\, dt\right] \tag{30}$$

Where $\tilde{Z}(t)\ and\ \widetilde{S_i}(t)^*$ define the complex envelop signal of $z(t)$ received and the ith data sequence with complex envelop respectively.

Substituting Laurent Decomposition expression (18) in (30) leads to the next metric (31):

$$\Lambda_{\mathrm{i}} = \sqrt{2Pt}\sum_{n=0}^{N-1}\lambda_i\,(n) \tag{31}$$

Where $\lambda_i(n)$ is defined as:

$$\lambda_i(n) = Re\left\{\sum_{K=0}^{2^{L-1}-1}\tilde{a}_{K,n}^{i} * \int_{-\infty}^{\infty}\tilde{Z}(t)C_k(t-nTb)\,dt\right\} \triangleq Re\left\{\sum_{K=0}^{2^{L-1}-1}\tilde{a}_{K,n}^{i} * r_{K,n}\right\} \tag{32}$$

i.e., the trellis branch metric, where $\tilde{a}_{K,n}^{i}$ are the ith, N length, complex data symbols associated to the data signal $s_i(t)$. Moreover, in order to compute every metric, exists an imposition reflected in (32), on which demands the knowledge of every $\tilde{a}_{K,n}^{i}$ which as it is shown in (25) and (26) depends on a number of states and current symbol.

In order to simplify the equality notation, it can be seen that $\int_{-\infty}^{\infty}\tilde{Z}(t)C_k(t-nTb)\,dt$ is the correlation value done at the output of the matched filters with the complex envelop noisy signal received.

Hence, $r_{K,n}$ denotes, that for each one of the 2^{L-1} filters fed simultaneously by the complex signal input ,by sampling the output at a nTb rate we can get a sufficient statistic for any fixed n that will serve to perform the decision.

3.2.1.3. Simplified VA Receiver: Kaleh's Receiver

The complexity of the optimum receiver resides in the fact that as shows Laurent Decomposition, the signal is formed by a large number of amplitude pulse modulation components.

During the explanation of Laurent Decomposition, it was explained that the first two amplitude modulation pulses $C_0(t)$ y $C_1(t)$ contain more than 99.999% of the total energy signal, thus, it allows us to reduce signal complexity by approximate it through only these pulses. Hence, pulses $\{C_k(t);\ K \le k \le 2^{L-1}-1; K=2\}$ are negligible since contain a very small percentage of the energy and the complexity of VA reduces to K filters and

$\tilde{a}_{K,n}^{i}$ with $k = K, K+1 \ldots, 2^{L-1}-1$ are not considered by the algorithm.

As such, applying the above consideration to (18), it can be approximated and rewritten as:

$$\begin{aligned}\hat{S}(t) &= \sqrt{2 \cdot Pt} \sum_{k=0}^{\hat{K}-1} \left[\sum_{n=-\infty}^{\infty} e^{i \cdot \frac{\pi}{2} A_{k,n}} \cdot C_k(t - nTb) \right] \\ &\triangleq \sqrt{2 \cdot Pt} \left[\sum_{n=-\infty}^{\infty} e^{i \cdot \frac{\pi}{2} A_{0,n}} \cdot C_0(t - nTb) + \sum_{n=-\infty}^{\infty} e^{i \cdot \frac{\pi}{2} A_{1,n}} \cdot C_1(t - nTb) \right], \hat{K} = 2\end{aligned} \tag{33}$$

The resulting receiver is depicted in the scheme given in Fig. 3-46:

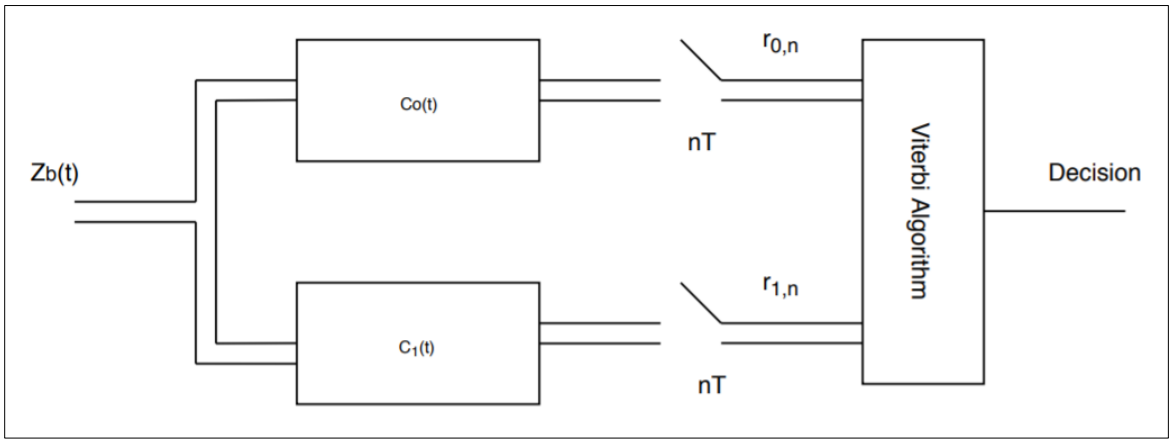

Figure 3-46: Simplified Viterbi Receiver

Likewise, $\tilde{a}_{0,n}^{i}, and\ \tilde{a}_{1,n}^{i}$ are determined through (25) and since the actual data symbols range over ± 1, then the even and odd complex symbols for each of the two pulse streams take on values:

$$\begin{aligned} \{\tilde{a}_{0,2n}\} \in \{j, -j\}, \quad & \{\tilde{a}_{0,2n+1}\} \in \{1, -1\} \\ \{\tilde{a}_{1,2n}\} \in \{1, -1\}, \quad & \{\tilde{a}_{1,2n+1}\} \in \{j, -j\} \end{aligned} \tag{34}$$

Then, through simple manipulation and assuming (34) for (25) we get to:

$$\begin{cases} \tilde{a}_{0,n} = j a_n \tilde{a}_{0,n-1} \\ \tilde{a}_{1,n} = j a_n \tilde{a}_{0,n-2} \end{cases} \tag{35}$$

In accordance with these approximations [7], the branch metrics computed by the simplified receiver are:

$$\hat{\lambda}_i(n) = Re\left\{ \sum_{k=0}^{\hat{K}-1} \tilde{a}_{K,n}^{i} * \int_{-\infty}^{\infty} \hat{\tilde{Z}}(t) C_k(t - nTb)\, dt \right\} \triangleq Re\left\{ \sum_{k=0}^{\hat{K}-1} \tilde{a}_{K,n}^{i} * r_{K,n} \right\} \tag{36}$$

Where $\hat{\lambda}_i(n)$ and $\hat{\tilde{Z}}(t)$ are the simplified metrics and complex envelop received signal taking into account $K = 2$ amplitude modulation pulses.

Also, the number of states of the VA is reduced, passing from 2^L to $2\widehat{K}$. **[8]**

So, based on these statements, metrics can be written as:

$$\hat{\lambda}_i(n) = Re\{\tilde{a}^i_{0,n} * r_{0,n} + \tilde{a}^i_{1,n} * r_{1,n}\} \tag{37}$$

And assuming even and odd parts, we thus get:

$$\hat{\lambda}_i(2n) = Re\{r_{0,2n}\} \cdot a^i_{2n} - Im\{r_{1,2n}\} \cdot a^i_{2n-2} a^i_{2n-1} a^i_{2n} \tag{38}$$

$$\hat{\lambda}_i(2n-1) = Im\{r_{0,2n-1}\} \cdot a^i_{2n-1} - Re\{r_{1,2n-1}\} \cdot a^i_{2n-3} a^i_{2n-2} a^i_{2n-1} \tag{39}$$

Where $a^i_{2n-2} a^i_{2n-1}$ and $a^i_{2n-3} a^i_{2n-2}$ are the 2 previous real bits of even and odd branch respectively which result in a four-state trellis shown in Fig. 3-47.

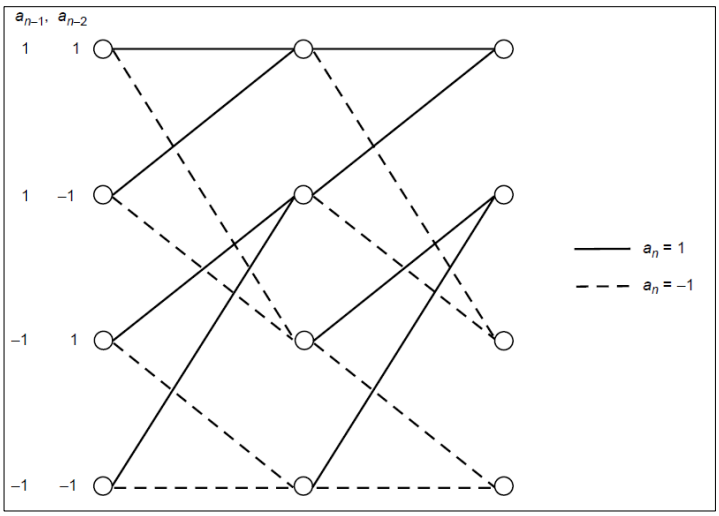

*Figure 3-47: Four-state trellis for a simplified VA **[8]***

Finally, the VA makes decisions on $\hat{a}_n$, and then a different decoder gives the related a_n symbols by applying the following rule:

$$\hat{a}_{2n} = -\hat{a}_{2n}\hat{a}_{2n-1}$$
$$\hat{a}_{2n+1} = \hat{a}_{2n+1}\hat{a}_{2n} \tag{40}$$

3.2.2. Ranging Receiver

3.2.2.1. Code Sequence Properties

The main property from which the design of our ranging receiver is derived, is the correlation between the different components that compose the signal.

Basically, our ranging system will work with two correlation values, In-Phase and Out-of-phase correlation.

In one hand, the in-phase value is produced when the signal is aligned with the complete sequence, while in the other hand, the out-of-phase value is produced when the component is shifted from 1 to $L_k -$, whose length is defined by L_k $(for\ K = 1,2, \dots ,6)$ and thus, non-aligned with the complete signal

A table with the In-Phase and Out-of-phase values is presented for both the T2B and the T4B sequence. These values have been calculated with a length equal to that of the total generated PN sequence of $1.009.470$ chips **[4]:**

*Table 6: In-Phase and Out-of-phase Correlation **[4]***

	T_4B In-Phase	T_4B Out-of-Phase	T_2B In-Phase	T_2B Out-of-Phase
C_1	947566	-947566	633306	-633306
C_2	61094	-10368	247020	-41404
$C_3\ Inverted$	61094	-6160	250404	-24900
$C_4\ Inverted$	61094	-4400	251332	-17852
C_5	61094	-3456	251604	-14056
$C_6\ Inverted$	61094	-2800	251940	-11388

As explained in 2.5.2 (Code Imbalance), 3 of the 6 sequence components are inverted in order to reduce the imbalance between +1 and -1 and so, reduce DC components, that are completely unnecessary.

From this property, the main operation of our receiver can be deduced, whose decision method will be based on calculating correlations and as reflected in the table with the correlation values, deciding which of the components and all its variants are aligned in the exact moment at which the reception system begins to acquire the PN sequence

3.2.2.2. Correlators

From the properties mentioned, the main operation of our receiver can be deduced, whose decision method will be based on calculating correlations and as reflected in the Table 6, deciding which of the components and all its variants are aligned in the exact moment at which the reception system begins to acquire the PN sequence.

Starting from the ranging signal acquired in the demodulation process, the latter will pass to a bank of correlators as it is shown in Fig. 3-48:

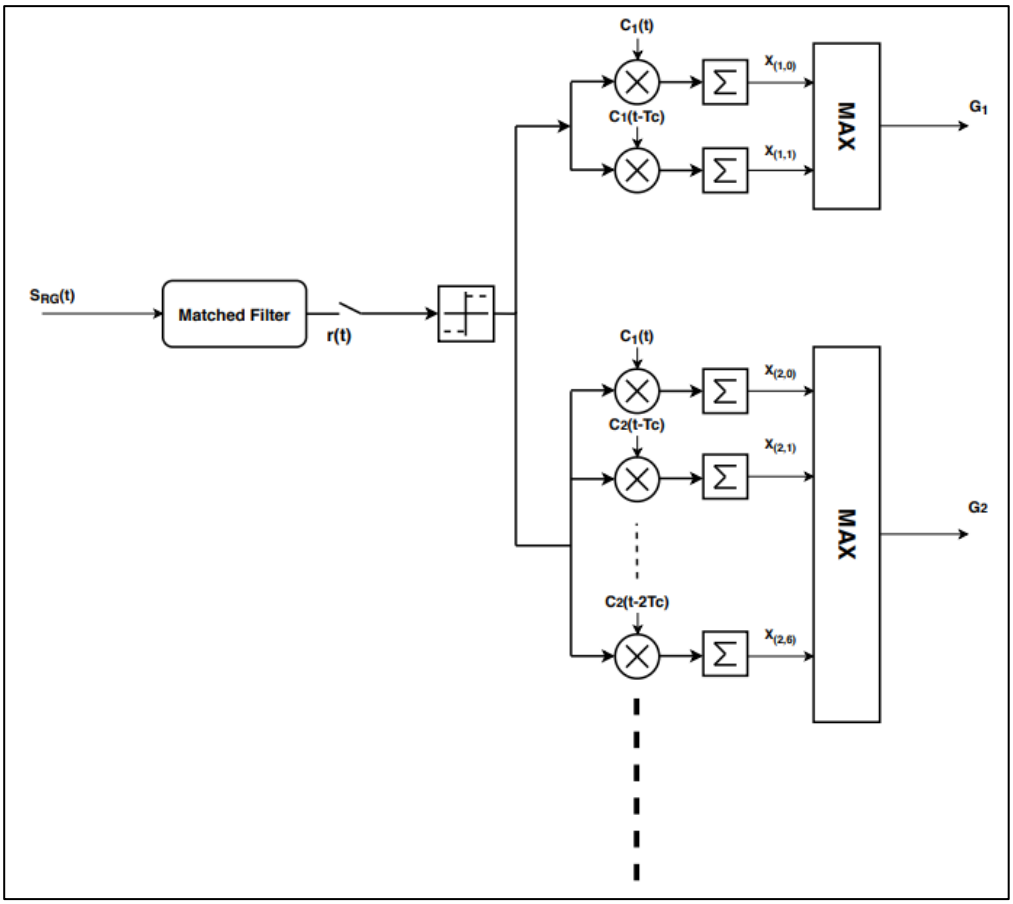

Figure 3-48: Bank of correlators

Each of these correlators as shown, will be responsible for working with each of the 6 components C_K and their respective shifts, resulting in:

Table 7: C2 Sequence and respective shifts

C_2 – Original Component	$1, 1, 1, -1, -1, 1, -1$
C_2 - Shifted L = 1	$1, 1, -1, -1, 1, -1, 1$
C_2 - Shifted L = 2	$1, -1, -1, 1, -1, 1, 1$
C_2 - Shifted L = 3	$-1, -1, 1, -1, 1, 1, 1$
C_2 - Shifted L = 4	$-1, 1, -1, 1, 1, 1, -1$
C_2 - Shifted L = 5	$1, -1, 1, 1, 1, -1, -1$
C_2 - Shifted L = 6	$-1, 1, 1, 1, -1, -1, 1$

As explained in the previous point, when performing the correlation with each of the L_k components, if the detected PN sequence is aligned with any of these components, a correlation value equal to that of In-phase corresponding to table 6 will be obtained. On the other hand, with the remaining $L_k - 1$ components the value obtained will be theoretically lower and equal to the Out-of-phase.

Once all the correlation values are obtained, the maximum of these will be chose between each of the banks. Likewise, this value will be directly associated with the sequence that will be chosen from among the possible combinations.

3.2.2.3. Remainder Theorem

The generation of the ranging signal does not go beyond being a module operation as illustrated in Fig. 2-4.

As just explained, a value will be obtained from each correlator that will act as the decision rule.

In accordance with the nomenclature shown in Fig. 3-48, the acquired value is directly related to the different components and their length as follows:

$$G_1 = \max\left(X_{1,0}, X_{1,1}\right)_{mod\ 2}$$

$$G_2 = \max\left(X_{2,0}, X_{2,1}, X_{2,2}, X_{2,3}, X_{2,4}, X_{2,5}, X_{2,6}\right)_{mod\ 7}$$

In general:

$$G_K = \max\left(X_{K,0}, X_{K,1} \ldots\ldots\ldots\ldots\ldots\ldots\ldots\ldots\ldots\ldots, X_{K,K-1}\right)_{mod\ K}$$

These values will be the inputs needed in order to guess at which position X_N the receiver started to acquis the signal of length N.

0 ..... N

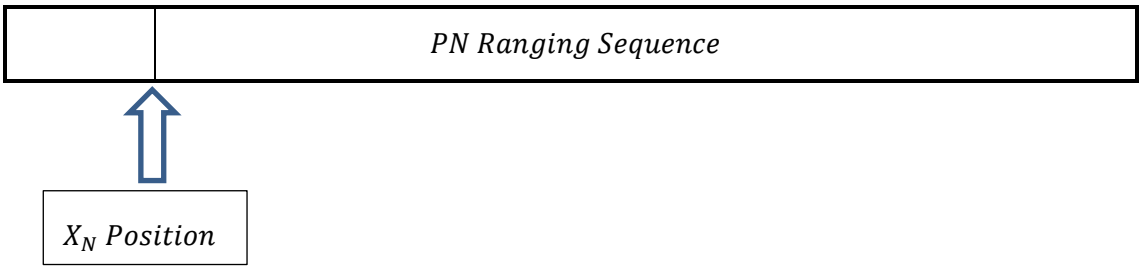

The algorithm that will be in charge to compute the mentioned parameter is the named Remainder Theorem, also called Chinese Remained Theorem [14][15].

The theorem establishes that having a base formed by prime numbers and pairwise coprime, these being in our case **2, 7, 11, 15, 19 and 23**, then for given integers $\boldsymbol{G_1}$, $\boldsymbol{G_2}$, $\boldsymbol{G_3}$, $\boldsymbol{G_4}$, $\boldsymbol{G_5}$ **and** $\boldsymbol{G_6}$, exists an X_N value that solves the following system:

$$\begin{cases} X_N = \boldsymbol{G_1}\, mod_2 \\ X_N = \boldsymbol{G_2}\, mod_7 \\ X_N = \boldsymbol{G_3}\, mod_{11} \\ X_N = \boldsymbol{G_4}\, mod_{15} \\ X_N = \boldsymbol{G_5}\, mod_{19} \\ X_N = \boldsymbol{G_6}\, mod_{23} \end{cases} \quad (41)$$

Moreover, X_N is a unique and congruent solution modulo the product of the basis $N = \mathbf{2 \cdot 7 \cdot 11 \cdot 15 \cdot 19 \cdot 23}$ **.**

In order to solve this congruence system, the algorithm follows the next steps [14][15]:

1. Compute modulo $N = 7 \cdot 11 \cdot 15 \cdot 19 \cdot 23 = 1.009.470$
2. Calculate: $y_1 = \frac{N}{2},\ y_2 = \frac{N}{7},\ y_3 = \frac{N}{11},\ y_4 = \frac{N}{15},\ y_5 = \frac{N}{19},\ y_6 = \frac{N}{23}$
3. Calculate: $z_1 = {y_1}^{-1} mod_2,\ z_2 = {y_2}^{-1} mod_7,\ z_3 = {y_3}^{-1} mod_{11},\ z_4 = {y_4}^{-1} mod_{15},\ z_5 = {y_5}^{-1} mod_{19},\ z_6 = {y_6}^{-1} mod_{23}$
4. The integer $X_N = \sum_{i=1}^{6} G_1 z_1 y_1 \cdot G_2 z_2 y_2 \cdot G_3 z_3 y_3 \cdot G_4 z_4 y_4 \cdot G_5 z_5 y_5 \cdot G_6 z_6 y_6$ is a solution of the system of congruences and X_N is the unique solution modulo N.

3.2.2.4. Ranging Receiver

The receiver presented below is responsible for the acquisition of the ranging signal through the processes explained in the last points and whose blocks are represented in Fig. 3-49.

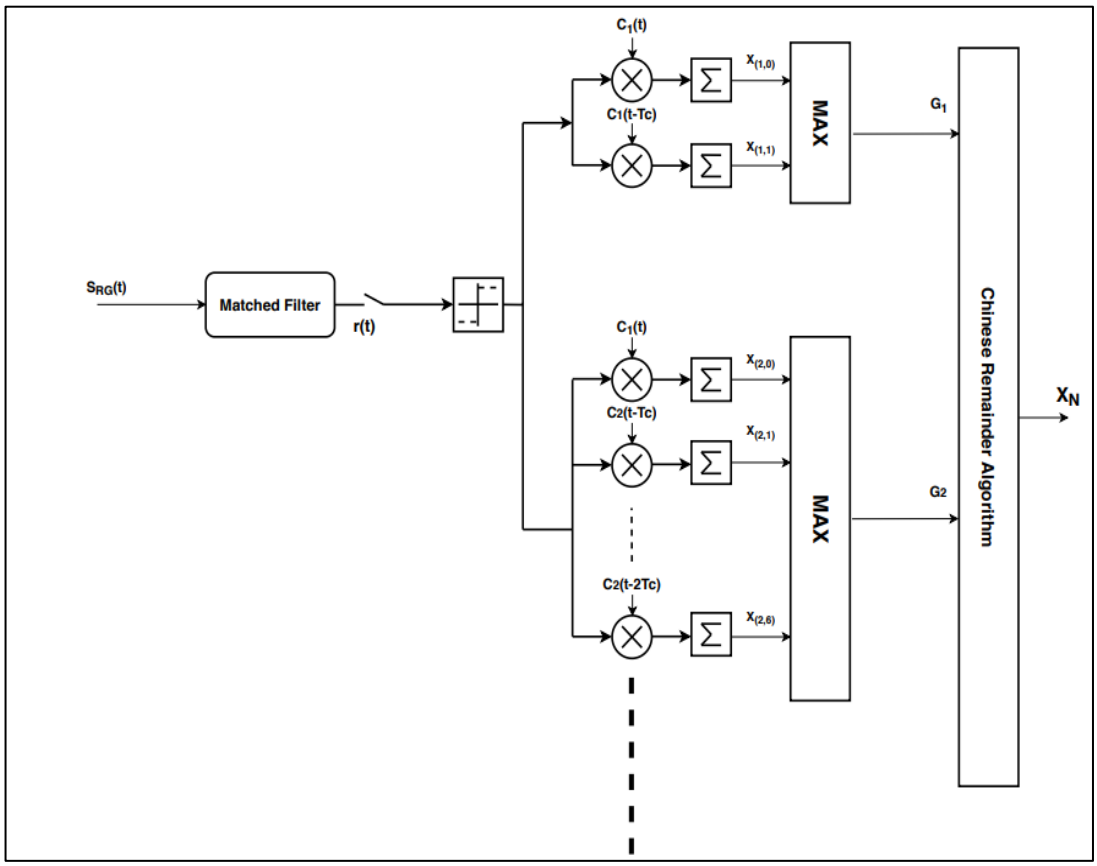

Figure 3-49: Ranging Receiver

In summary and as an end point, the complete operation of this ranging receivers is described next.

The noisy ranging signal received (previously demodulated in phase) $S_{RG}(t)$ passes through the adapted filter (14) and then is sampled every Tc.

These bits, which build the chip sequence to be acquired, are passed through the filter bank.

Next, the value obtained at the output of the different correlators, as explained in section **3.2.2.3**, form the values that will generate the congruence system to be solved by the C.R.T as described.

The result of this last process will define the position from which our receiver began to receive the ranging sequence and therefore, knowing the components by which this ranging signal is formed, we can regenerate the entire signal.

3.2.3. Simultaneous Telemetry and PN Ranging receiver

3.2.3.1. Receiver without Ranging Cancellation

Once the receivers that will take care of the corresponding telemetry and ranging signals have been presented, the reception scheme that will be used for the reception of the combined range and telemetry signal is introduced.

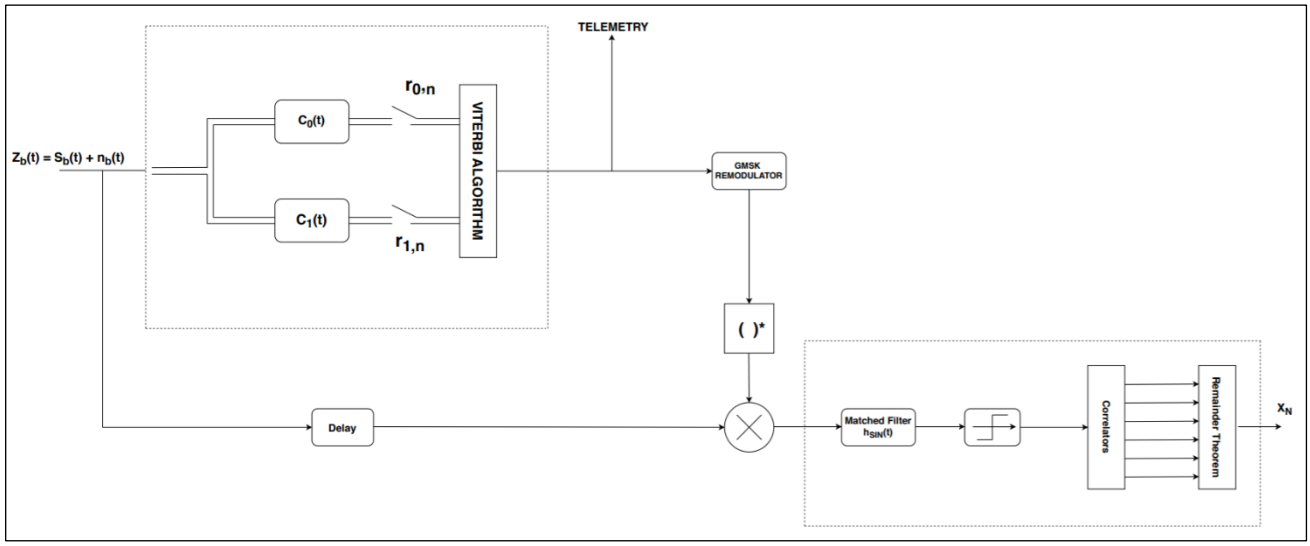

Figure 3-50: Receiver Schematic for GMSK + PN Ranging

The operation of the telemetry and ranging blocks follow the same operation described previously. Regarding the functioning and followed by the global scheme, which is aimed at receiving the combined telemetry and ranging signal are explained next.

The first phase consists of demodulating and detecting the telemetry from the combined signal $Z_b(t)$. The telemetry signal will be affected by more or less interference due to the ranging, being the latter more impactful as the ranging index increases defined by the m_{RG} parameter.

The detected telemetry symbols acquired through Laurent-Viterbi processing, will be remodulated into a GMSK format, regenerating the telemetry signal and subsequently conjugating it and resulting in the complex envelop signal $\left(e^{i\cdot\varphi_{RG}(t)}\right)^*$. Then, as a small delay had been applied to the entire branch below as illustrated in the diagram, the remodulated signal is used to eliminate the GMSK from the composite signal and ideally only the ranging signal remains as follows:

$$\begin{aligned} Z_b(t)\cdot(e^{i\cdot\varphi_{TM}(t)})^* &= (S_b(t)+n_b(t))\cdot(e^{i\cdot\hat{\varphi}_{TM}(t)})^* \\ &= \left(e^{i\cdot\varphi_{TM}(t)}e^{i\cdot\varphi_{RG}(t-\tau_{RG})}+n_b(t)\right)\cdot\ e^{-i\cdot\hat{\varphi}_{TM}(t)} \\ &= e^{i\cdot\varphi_{TM}(t)}e^{-i\cdot\hat{\varphi}_{TM}(t)}e^{i\cdot\varphi_{RG}(t-\tau_{RG})}+\hat{n}_b(t) \end{aligned} \quad (42)$$

Assuming an ideal synchronization case and depending on whether telemetry has been detected in a better or worse way, we can find different scenarios.

In the best detection case, the signal got at the input of the ranging demodulator will be free of telemetry and therefore, enhances the ranging receiver and improving the acquisition of the sequence.

$$Z_b(t) \cdot \left(e^{i\cdot\varphi_{TM}(t)}\right)^* = e^{i\cdot\varphi_{RG}(t-\tau_{RG})} + \hat{n}_b(t) \qquad (43)$$

Otherwise, if the detected telemetry signal was not optimal, we would have a ranging signal combined with an additional residual telemetry signal (42).

In addition, the noise at the entrance in both cases, would be a rotated Gaussian noise $\hat{\boldsymbol{n}}_{\boldsymbol{b}}(\boldsymbol{t})$, i.e., the characteristics in terms of variance and mean remain identical so there's no noise enhancing.

Next, ranging signal passes through a matched filter $\boldsymbol{h_{sin}(t)}$ and then is processed analogously as in **3.2.2.4** getting the position from which the system began to receive the PN sequence.

3.2.3.2. Receiver with Ranging Cancellation

One of the new updates recently introduced in standard, as indicated in section 2, suggests an alternative receiver which focuses on the implementation of a ranging cancellation system **[3].**

The following Fig. 3-51 illustrates how the system would work.

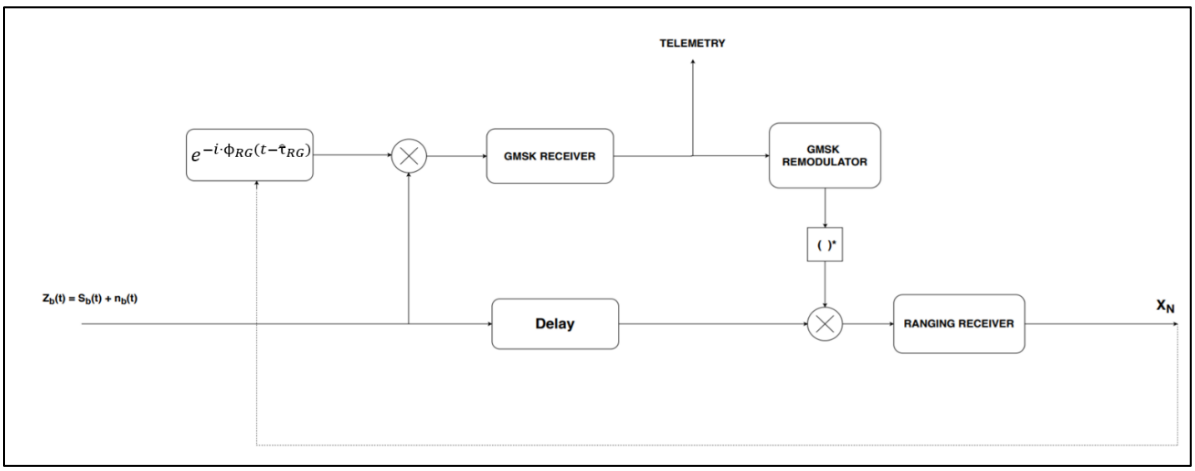

Figure 3-51: Receiver Diagram with Ranging Cancellation

Basically, this system approaches in a similar way, the removal of the ranging signal before telemetry demodulation.

Once the ranging receiver, concretely the correlators, have locked-in the delay parameter, the system is ready to cancel the raging signal.

As the different components are perfectly known a priori, the delay X_N is enough to regenerate the RG Signal. The RG regenerator generates a complex conjugated envelop signal which analogously as the telemetry cancellation works, will serve to remove the ranging signal from the composite one.

In summary, it's a system whose primary objective is to enhance the telemetry detection in case ranging (acting as an interference) impacts strongly the composite signal and thus, GMSK performance.

Analytical model of RG Cancellation is defined by (44):

$$\begin{aligned} Z_b(t) \cdot (e^{i\cdot\varphi_{RG}(t)})^* &= (S_b(t) + n_b(t)) \cdot (e^{i\cdot\hat{\varphi}_{RG}(t-\hat{\tau}_{RG})})^* \\ &= \left(e^{i\cdot\varphi_{TM}(t)} e^{i\cdot\varphi_{RG}(t-\tau_{RG})} + n_b(t)\right) \cdot e^{-i\cdot\hat{\varphi}_{RG}(t-\hat{\tau}_{RG})} \\ &= e^{i\cdot\varphi_{TM}(t)} e^{i\cdot\varphi_{RG}(t-\tau_{RG})} e^{-i\cdot\hat{\varphi}_{RG}(t-\hat{\tau}_{RG})} + \hat{n}_b(t) \end{aligned} \quad (44)$$

Where, if $\hat{\tau}_{RG}$ is an accurate estimation ($\hat{\tau}_{RG} = \tau_{RG}$) then:

$$Z_b(t) \cdot (e^{i\cdot\varphi_{RG}(t)})^* = Z_{RG_{Cancel}}(t) = e^{i\cdot\varphi_{TM}(t)} + \hat{n}_b(t) \quad (45)$$

Therefore, with this simple RG cancellation process, the TM degradation due to the simultaneous GMSK + PN RG approach is completely eliminated.

Only in the case of an imperfect RG delay estimation ($\hat{\tau}_{RG} \neq \tau_{RG}$), this could generate some degradation due $e^{i\cdot\varphi_{RG}(t-\tau_{RG})} e^{-i\cdot\hat{\varphi}_{RG}(t-\hat{\tau}_{RG})}$ factor.

4. Results

This section analyses the results obtained from the simulation of each block that composes our receiver.

Initially, the results concerning the Ranging and Telemetry receivers will be presented. Subsequently, the results obtained from the simulation of the complete reception scheme will be studied, where the impact of each of the signals with respect to the other will be analysed through key parameters, such as the time-bandwidth product, ranging index modulation etc. Moreover, effects of an asymmetrical ratio between telemetry and ranging rate will be illustrated.

Then we will present the simulations in which the range cancellation system is applied and demonstrate the advantage that supposes its implementation.

4.1. PN Ranging Receiver

Starting from the ranging receiver, it was presented a system based on a bank of correlators next to a Remainder Algorithm block (see Fig. 3-49), in order to lock up the ranging delay at the reception path.

As it was explained, basically the CCSDS recommends two alternatives called T_2B and T_4B, whose main difference appears in the construction, giving different votes on the clock sequence C_1.

Next, Acquisition probability plots regarding both T_2B and T_4B are shown:

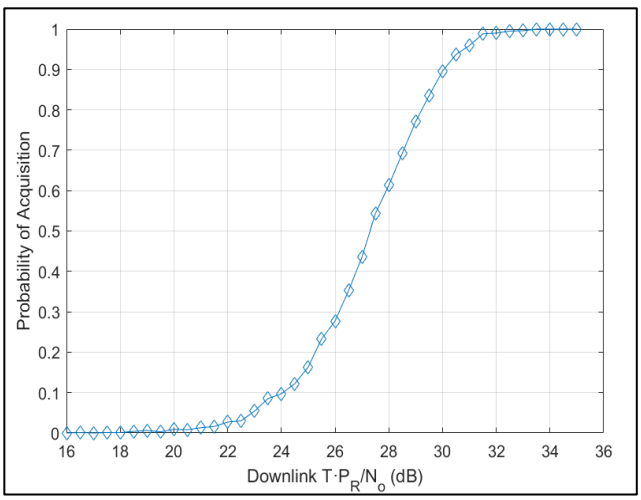

Figure 4-1: T2B Probability of Acquisition

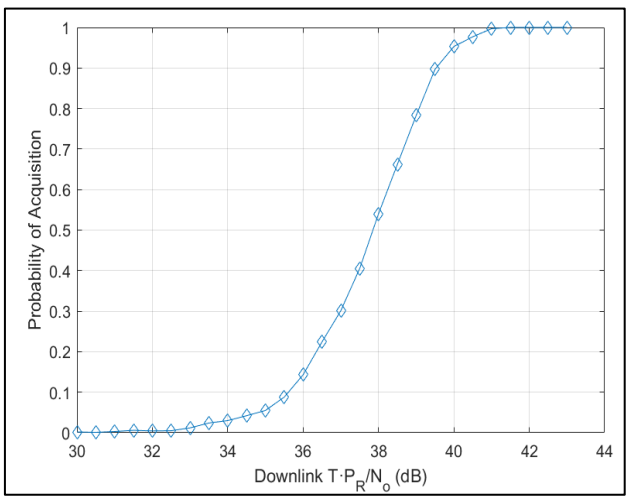

Figure 4-2: T4B Probability of Acquisition

In order to understand the plots, is it necessary to remind the two primary approaches regarding ranging, which are:

- Time Acquisition
- Accuracy

Codes that have been presented, are designed to meet one of these two requirements.

As it was seen in Ranging structure and generation section **(3.1.2),** Table 4 illustrates the in-phase and out-of-phase correlations between the whole generated sequence and each of the composite codes.

Analysing these values, it can be seen how the difference between them is greater in T_2B structure. Somehow, this suggests that the greater the difference between these values and taking into account that the algorithm on which the ranging receiver is based is a maximum search algorithm, raises the fact that it is easier for the algorithm to distinguish the aligned sequence from its L_K-1 shifts on each correlator block. Hence, the integration time needed in order to choose the most probable C_k component by the algorithm is lesser than in T_4B. At the same time, this implies that the probability of acquiring the sequence on a lower time is greater in T_2B, in case both types of codes work in the same conditions, such as in additive noise environment, E_bN_0 etc.

As an example, component C_6 correlation values are:

Table 8: C6 Correlation Values

	T_2B	T_4B
In Phase	251940	61094
Out of Phase	-11388	-2800

Then, if we define a parameter β as:

$$\beta = \frac{In\ Phase_{T2B} - Out\ of\ Phase_{T2B}}{In\ Phase_{T4B} - Out\ of\ Phase_{T4B}} \tag{46}$$

Particularizing the equation with the presented values, we get that $\beta \approx 4$, i.e., that the minimum difference between those values is 4 times greater in T_2B than in T_4B (worst case).

Then, the graphs presented in Figs. 4-1 and 4-2 demonstrate this fact, since as can be seen, using the sequence with less clock weight, signal acquisition starts at a lower SNR than in the other case.

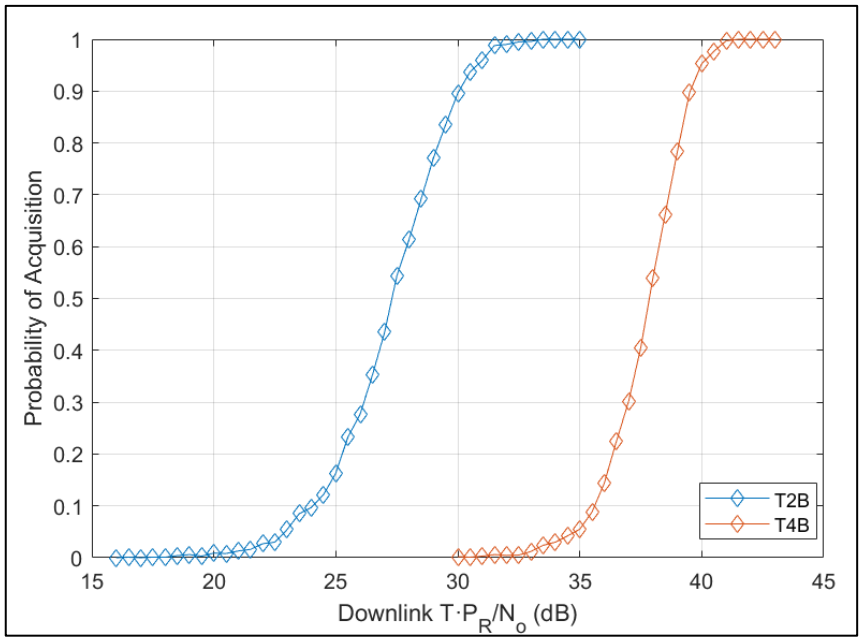

Figure 4-3: T4B Vs. T2B

The proposed parameter for the analysis is the $T \cdot \frac{Pr}{No}$ where T and Pr are the integration time and ranging power respectively**.**

This parameter allows us a double justification to the explained above. If we set a fixed E_bN_0 condition for both sequences, the second one needs a greater integration time to obtain an equal acquisition probability or likewise, if the same T is set, it needs a higher E_bN_0 level. In both cases, around 10 dB higher.

On the other hand, as far as precision is concerned, T4B is better because it has a much stronger clock than its alternative and this is directly related to the accuracy **[11][12].**

In summary, for deep space missions where signal reception conditions are poor and time acquisition is primary, T_2B is a better alternative, otherwise, if accuracy is needed to allocate the transmitter, T_4B is better **[11].**

4.2. Telemetry Receiver

The telemetry receiver proposed in the project consists of a simplified and therefore suboptimal version based on 2 Laurent filters and a 4-state Viterbi algorithm (see Fig. 3-45) but with benefits quite similar to those that we could obtain with the optimal receiver.

Below are the results obtained by simulating the reception of the GMSK shaped telemetry signal whose values are B·Tb = 0.25 and B·Tb = 0.5.

It should be noted that during the simulation in the case of B·Tb = 0.5 and as explained in the **3.2.1.1 (Laurent Expansion)** section, assuming a truncation of the pulse L inversely proportional to the value of B·Tb, therefore L = 2, the receiver did not work properly. The problem was solved by assuming a slightly lower truncation (more finite ISI) and therefore a slightly higher L. In this case, with an L = 3 or 4, it worked satisfactorily.

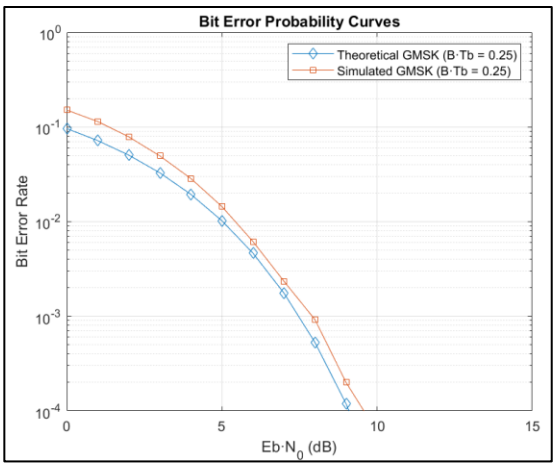

Figure 4-4: BER Curves for B·Tb = 0.25

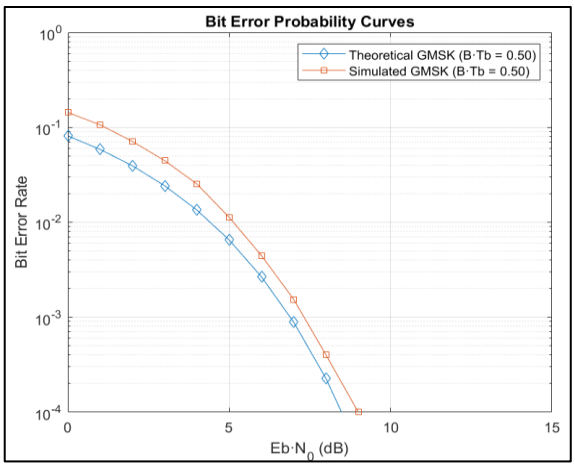

Figure 4-5: BER Curves for B·Tb = 0.50

Figs. 4-4 and 4-5 show the error probability curves obtained for both GMSK alongside their respective theoretical curve based on a bound provided by **[13],** which indicates approximately the ideal performance of a GMSK in coherent reception.

Theoretically, the behaviour of the B · Tb = 0.5 signal is better because the inherent ISI is lower. In addition, it is clear that our receiver does not have an ideal behaviour at all, since as we have emphasized it is a suboptimal version.

The losses in this case between the optimal and suboptimal case can be upper bounded for low SNR with an average value of **0.95 dB** while for high SNR values the curve tends slightly to the theoretical one with an average loss of **0.52 dB** for both cases.

Regarding the BER between the two simulated curves, for a fixed error probability, the gain needed in terms of E_bN_0 for the second curve corresponding to B·Tb = 0.25 is slightly higher for values of BER ≤ 10^{-2} corresponding to an average around **0.73 dB**.

Moreover, under low signal conditions, the improvement in terms of probability of error between the two signals is quite similar as it can be seen in Fig. 4-6.

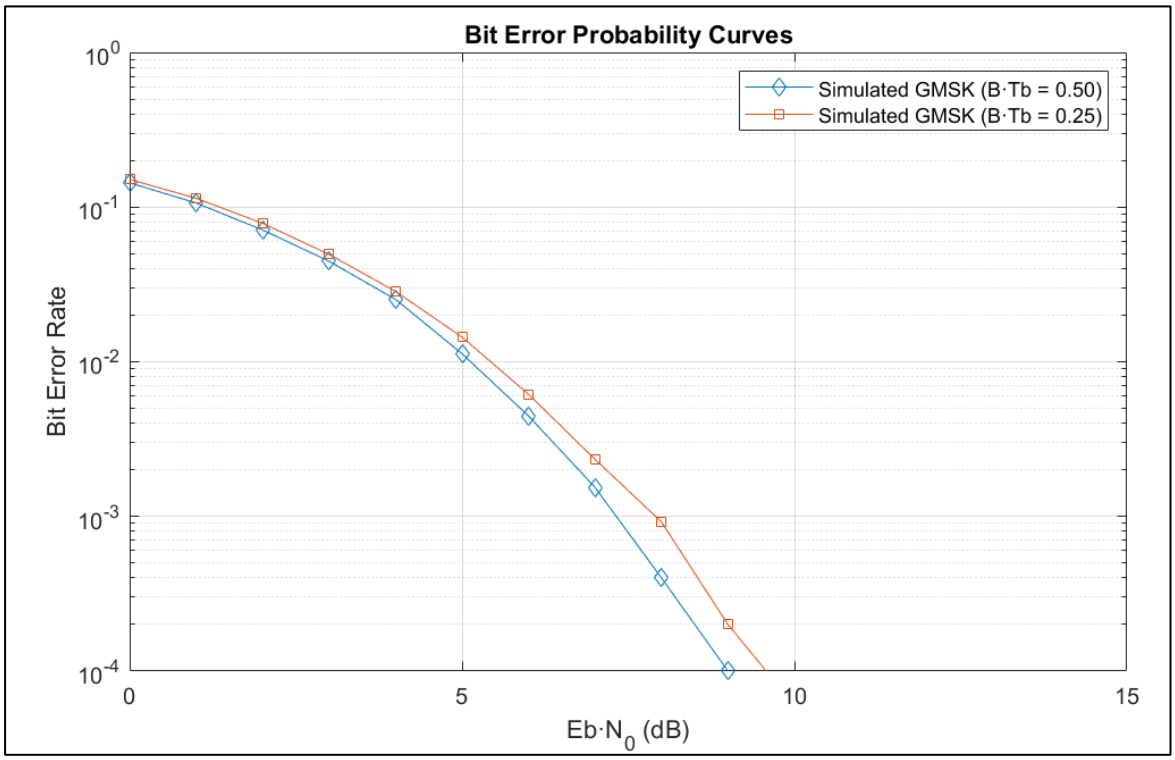

Figure 4-6: Simulated B·Tb = 0.25 GMSK's BER Vs. B·Tb = 0.5 GMSK's BER

In summary, the performance of the receiver in good SNR conditions will be averaged to **0.75 dB** below the optimal receiver performance. Its operation in the case of telemetry modelled as a GMSK of B·Tb = 0.5 will be slightly better than the other case due mainly to the reduced intrinsic ISI.

4.3. Complete Receiver

This section presents the simulation results of the PN Ranging + Telemetry receiver developed.

The different parameters that characterize both signals and the impact of each of these on the behaviour of the signal formed by both signals will be analysed through the plots.

In addition, two main cases will be seen. The first, based on the original system without ranging cancellation. The second, based on ranging cancellation.

4.3.1. Complete Receiver without Ranging Cancellation

The first case to study, as previously mentioned, consists on the original receiver scheme without ranging cancellation presented in **3.2.3.** (Simultaneous Telemetry and PN Ranging receiver) and illustrated in Fig. 3-50.

For this first scenario we will assume 2 situations under the same telemetry and ranging conditions:

1. For a ratio between ranging and telemetry rates of $\frac{R_{RG}}{R_{TM}} \cong 1$
2. For a ratio between ranging and telemetry rates of $\frac{R_{RG}}{R_{TM}} \geq 3$

For $\frac{R_{RG}}{R_{TM}} \cong 1$ the following graphs concerning telemetry and ranging have been obtained:

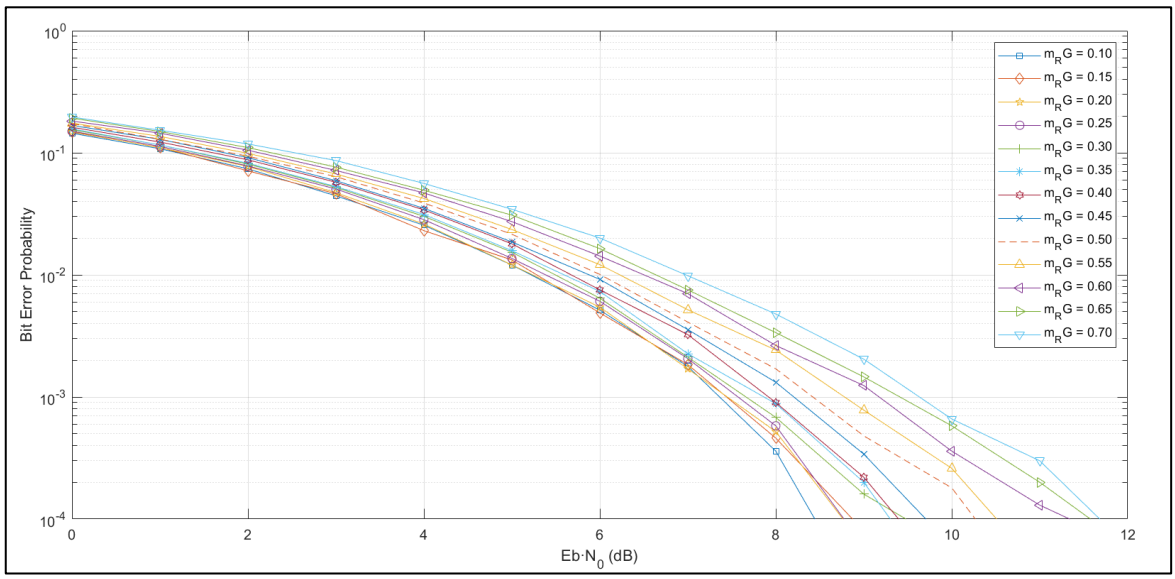

Figure 4-7: BER Curves for with different Ranging Indexes (B·Tb = 0.5, T2B)

Taking into account the different combinations that can be simulated, the main features of each one will be seen.

Starting with the telemetry sequence for B·Tb = 0.5, Figs. 4-7 and 4-9 represent error probability curves for telemetry signal and for different ranging modulation indexes (in steps of 0.5) m_{RG}. It can be seen that as the ranging index increases and as defined in equation (13), the impact of the ranging signal on the set is greater and therefore the error probability curves open indicating a worsening in the probability of telemetry detection.

Through analysis, choosing m_{RG} values greater than 0.45, benefits ranging and as a consequence it has a negative impact on the telemetry signal reflected on its BER curves, while choosing values under 0.45 benefits the telemetry.

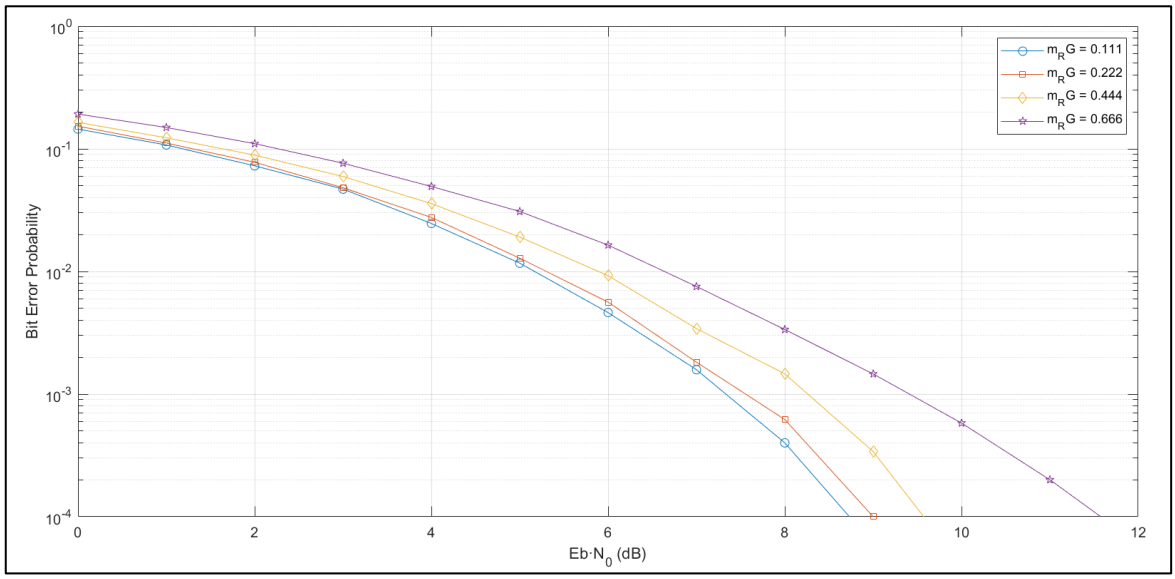

Figure 4-8: BER Curves for Key Ranging Index Values (B·Tb = 0.5, T2B)

Table 9: Ranging Impact on Telemetry.

	Necessary E_bN_0 to reach the targeted BER (dB)			
Target BER	m_{RG}= 0.111	m_{RG} = 0.222	m_{RG} = 0.444	m_{RG} = 0.666
10^{-2}	5.23	5.32	5.91	6.71
10^{-3}	7.22	7.52	8.31	9.35
10^{-4}	8.81	9.08	9.49	11.48

Table 9 presented above based on Fig. 4-8 illustrates the necessary E_bN_0 for a fixed m_{RG}.

The selected values are those indicated by the standard to characterize the signal that the system will generate.

It can be seen how the EbN_0 requirement for a fixed BER increases, especially for values greater than 0.444.

Furthermore, comparing qualitatively the worst case of both simulations, i.e., B·Tb = 0.5 and T2B, T4B with m_{RG} = 0.666 (see Figs.4-8 and 4-10), we can see a remarkable improvement at a glance of more than 1 dB for a fixed BER of 10^{-4}.

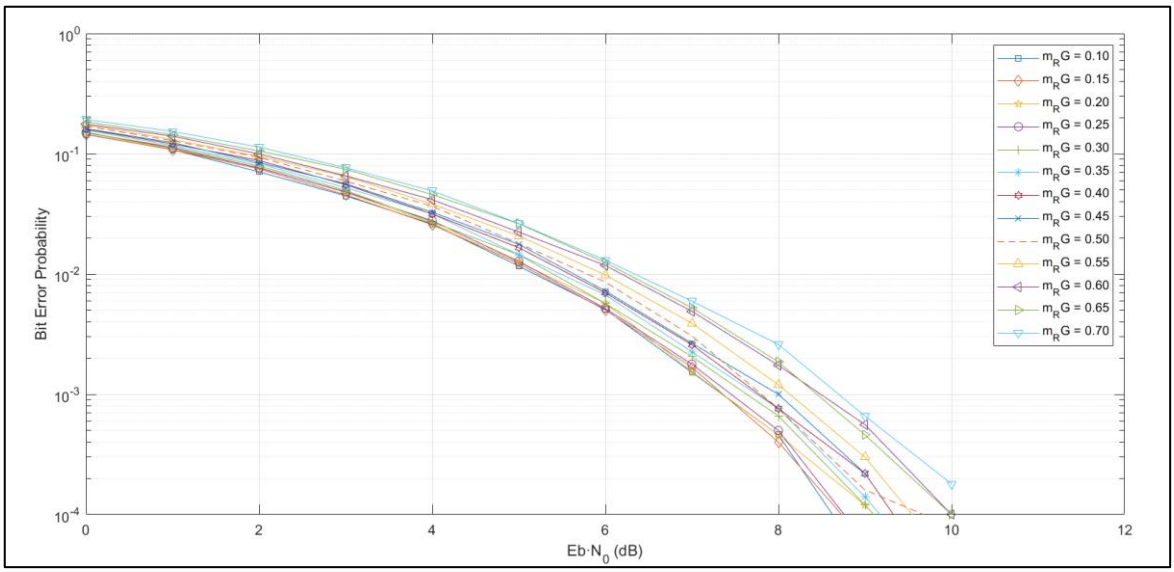

Figure 4-9: BER Curves for with different Ranging Indexes (B·Tb = 0.5, T4B)

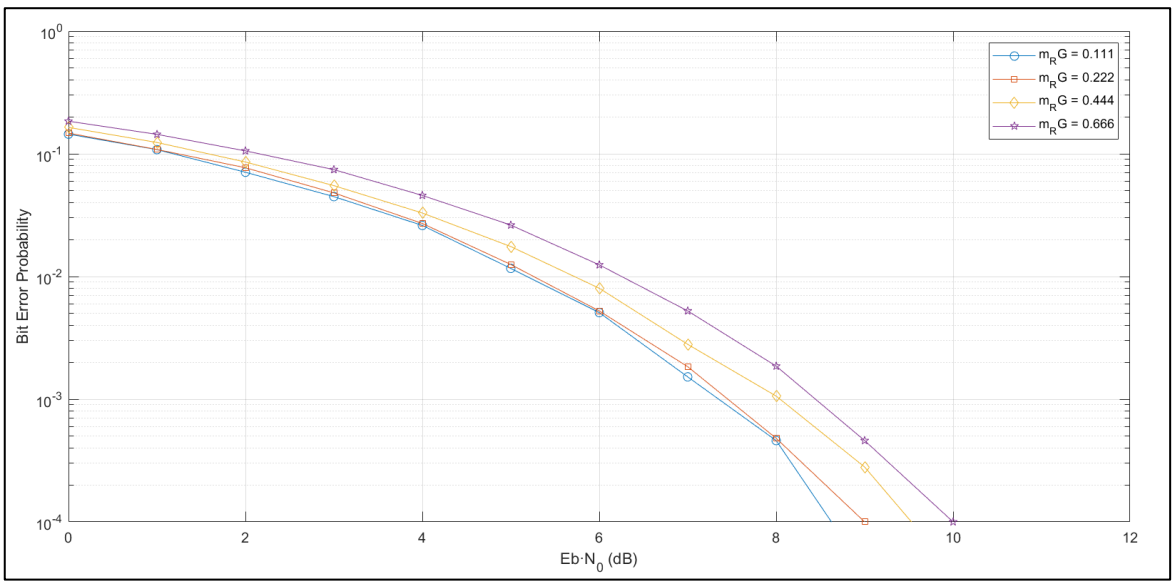

Figure 4-10: BER Curves for Key Ranging Index Values (B·Tb = 0.5, T4B)

Similarly, if the case B·Tb = 0.25 is simulated, we obtain the following plots for T2B and T4B shown in Figs. 4-11 and 4-12.

As for telemetry, we will obtain much more open curves due to the ISI increment. In general, the behaviour is the same as in the previous case when a ranging index increment is done.

Likewise, it can be seen how changing the type of ranging sequence affects the curves analogously to the previous case, that is, the T4B sequence is slightly better for indexes greater than 0.45.

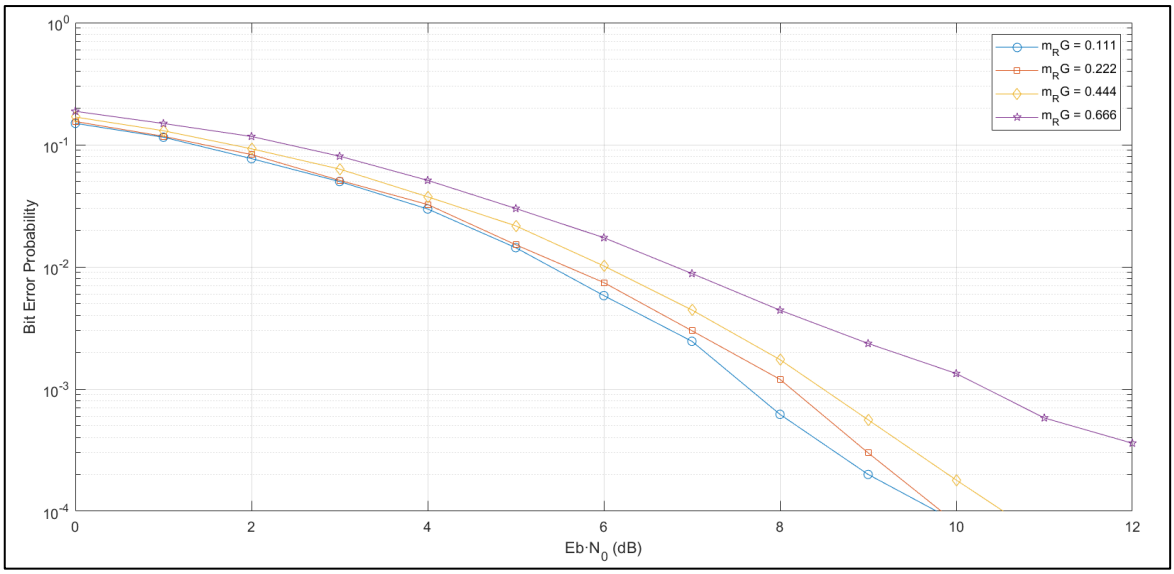

Figure 4-11: BER Curves for Key Ranging Index Values (B·Tb = 0.25, T4B)

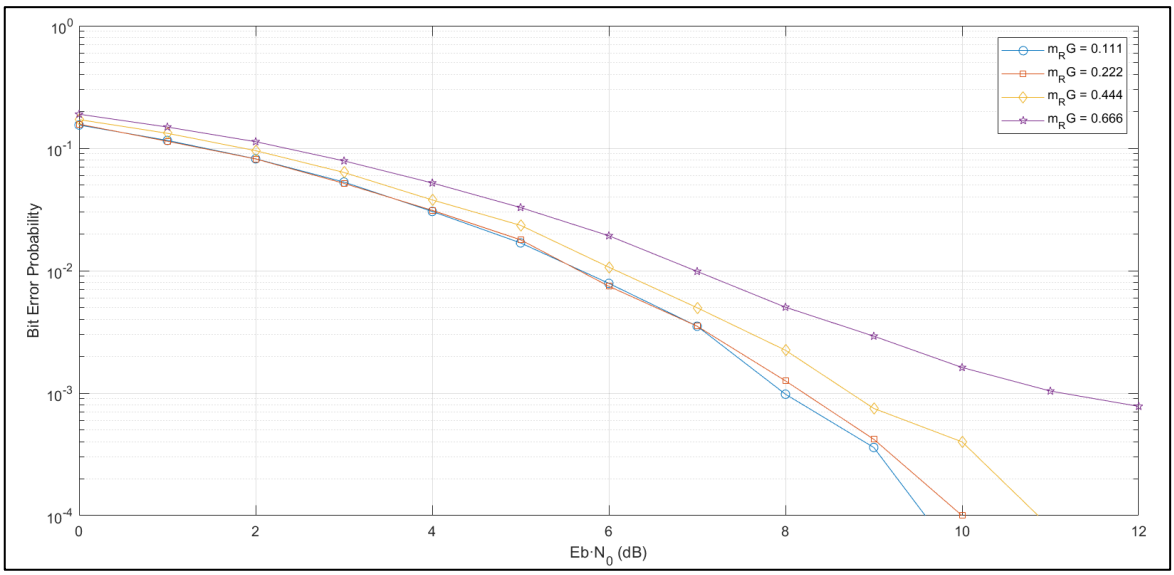

Figure 4-12: BER Curves for Key Ranging Index Values (B·Tb = 0.25, T2B)

In the other hand for $\frac{R_{RG}}{R_{TM}} \geq 3$ the following graphs concerning telemetry and ranging have been obtained. In this case we will focus mainly on the most important indexes highlighted by the standard CCSDS [0.111, 0.222, 0.444, 0.666].

As will be explained below, the fact that the imbalance between the rates could be way greater than 1 is beneficial for the performance of our system if only telemetry is concerned.

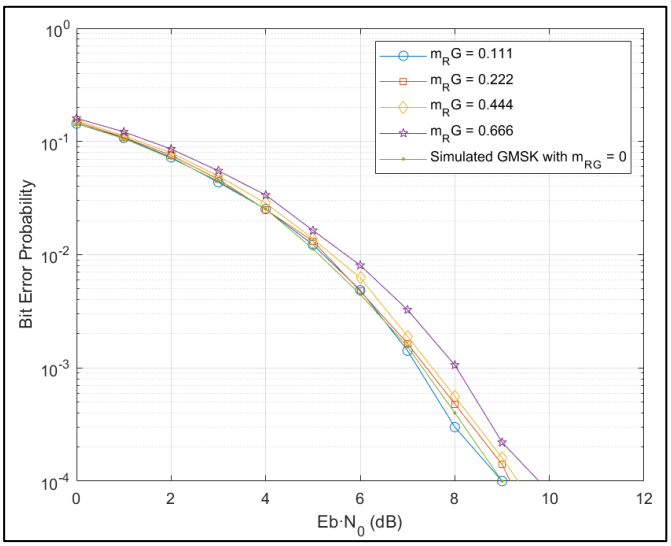

Figure 4-13: BER Curves for $\frac{R_{RG}}{R_{TM}} \geq 3$ case (B·Tb = 0.50, T2B)

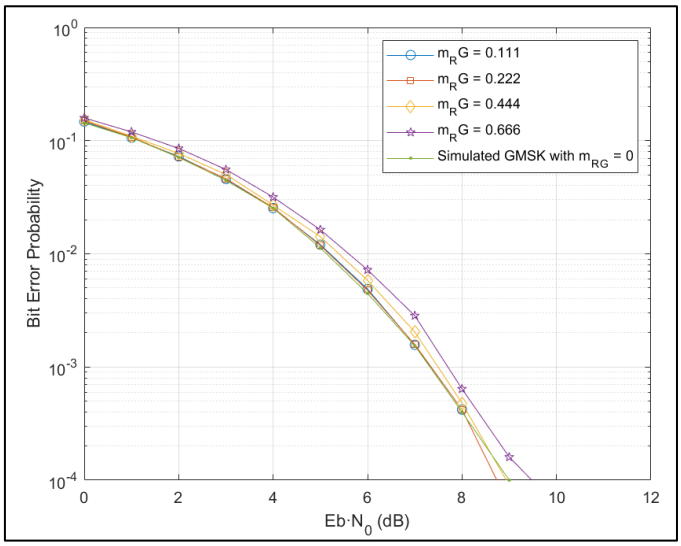

Figure 4-14: BER Curves for $\frac{R_{RG}}{R_{TM}} \geq 3$ case (B·Tb = 0.50, T4B)

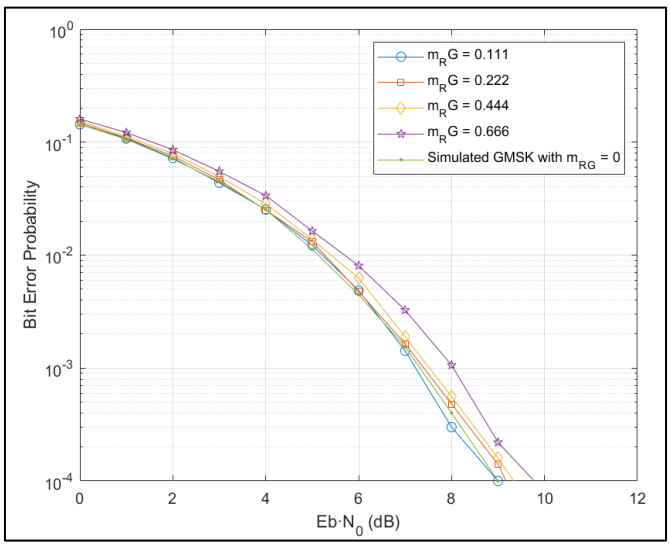

Figure 4-15: BER Curves for $\frac{R_{RG}}{R_{TM}} \geq 3$ case (B·Tb = 0.25, T2B)

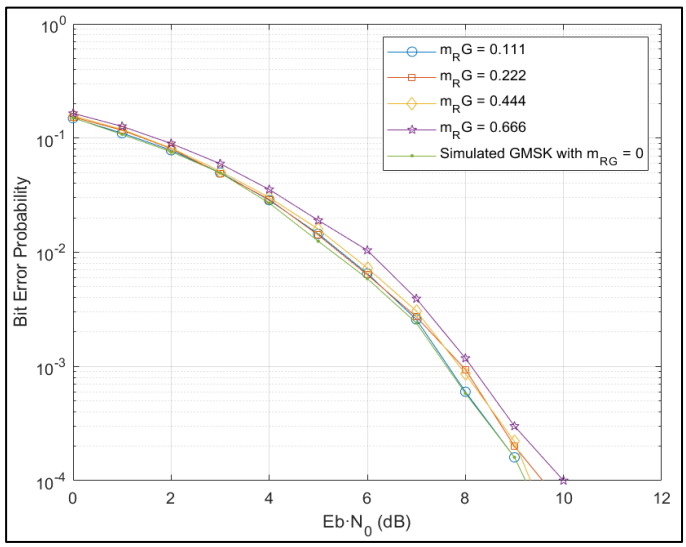

Figure 4-16: BER Curves for $\frac{R_{RG}}{R_{TM}} \geq 3$ case (B·Tb = 0.25, T4B)

Figs. 4-13, 4-14, 4-15 and 4-16 show all possible combinations between the parameters of ranging and telemetry alongside the curve which represented the BER for a pure GMSK processed with our receiver.

Starting from the case in which the telemetry rate is fixed, if the ranging rate increases then the orthogonality between these components decreases and therefore the interference between them as well. This is the case we're actually studying in this subsection.

On the contrary, if the ranging rate is fixed and the telemetry rate increases, then the probabilities that a telemetry bit is wrong during a chip interval increases and therefore the system performance is reduced. In addition, this implies that the ranging affects telemetry much more as the range index increases.

In these graphs, you can see how all the curves tend to the curve that does not consider the ranging (pure GMSK) and therefore an important improvement is achieved. Hence, it can be considered as the best case we can work with following the CCSDS standard restrictions if only telemetry is concerned.

4.3.2. Complete Receiver with Ranging Cancellation

In view of the results obtained in **(4.3.1)** simulation results, it's important to study the proposed approach in order to reduce the effects of ranging on the telemetry signal.

Figs. 4-17, 4-18, 4-19 and 4-20 show the improvement in terms of BER resulting from the application of a ranging cancellation explained in **3.2.3.2** (Receiver with Ranging Cancellation).

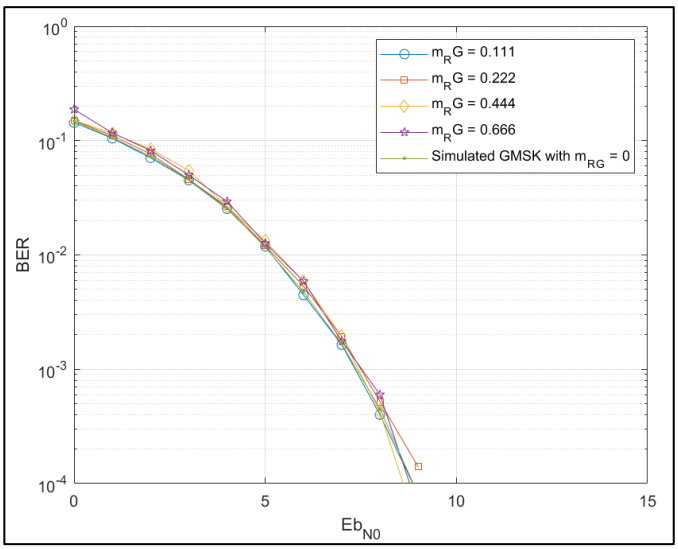

Figure 4-17: RG Cancellation to GMSK B·TB = 0.5 T4B

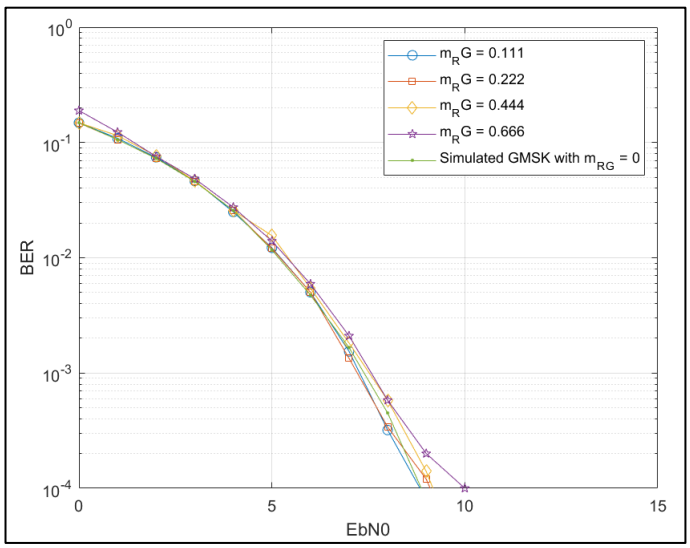

Figure 4-18: RG Cancellation to GMSK B·TB = 0.5 T2B

As can be seen, the ranging cancellation system works as predicted theoretically during the explanation in its corresponding section. We see how all the curves are very close to the ideal curve and therefore we have been able to overcome the effect of ranging interference greatly.

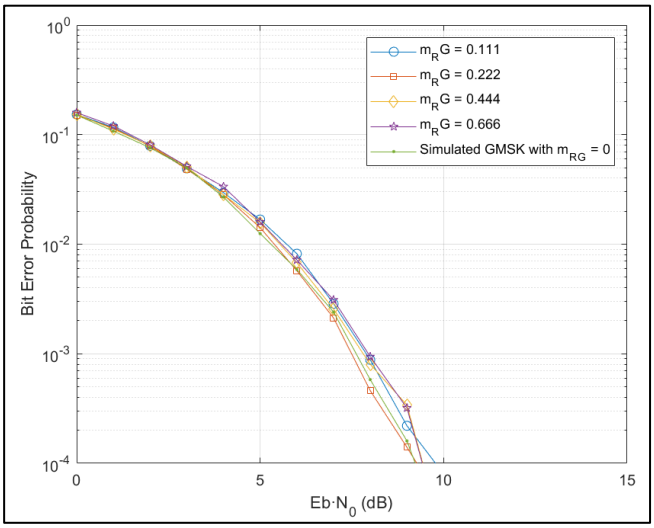

Figure 4-19: RG Cancellation to GMSK B·TB = 0.25 T2B

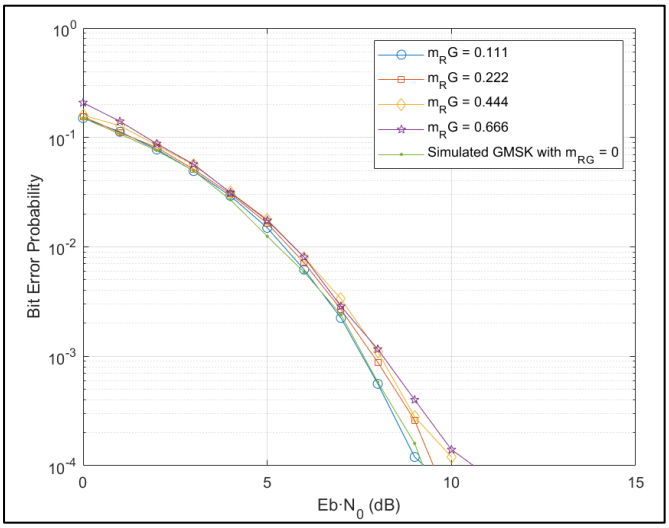

Figure 4-20: RG Cancellation to GMSK B·TB = 0.25 T4B

We have to take into account that there is a very important trade-off in terms of cancellation of ranging. Depending on the characterization of the signal, this will benefit us or not since if the ranging is very strong, it will greatly interfere with the detection of telemetry and therefore in the telemetry cancellation stage, we will add an interfering signal instead of eliminating the telemetry completely from the ranging signal. This case is illustrated in all plots above when ranging index is 0.666, not performing as good as for other ranging indexes but still improving the BER if compared to the case without ranging cancellation. This justifies the fact that even for an imperfect cancellation, exists an important improvement.

When a ranging index of 0.111 is used, RG cancellation is really unnecessary in terms of BER enhancement since it's not as impactful as 0.666.

In cases showed in Figs. 4-17 and 4-18, due low ISI attributes of the signal, the systems overperforms the NO-RG Cancellation cases.

In summary, Table 10 indicates the improvement in terms of BER if RG Cancellation is used and taking into account the worst case (m_{RG} = 0.666) for a given fixed BER of 10^{-3}.

Table 10: Ranging Cancellation Improvement.

B·Tb, T2B/T4B	m_{RG} = 0.666, BER of 10^{-3}
0.25, T2B	3,10 dB
0.25, T4B	2,41 dB
0.50, T2B	1,64 dB
0.50, T4B	1,13 dB

Finally, we will present tables to illustrate qualitatively if any improvement effect between E_bN_0 and Pacq is done compared to the case without RG Cancellation for a fixed

The study of the worst case in terms of Ranging and SNR will be considered, that is, code T4B with B · Tb = 0.5 / 0.25 which is the most SNR-dependent combination.

Table 11: EbN0 (dB) Needed to achieve a fixed Pacq (RG Cancellation)

	$B \cdot T_b = 0.25$, T_4B		$B \cdot T_b = 0.50$, T_4B	
P_{ACQ}	1%	100%	1%	100%
$m_{RG} = 0.111$	14	22	10	21
$m_{RG} = 0.222$	6	14	5	14
$m_{RG} = 0.444$	2	9	0	8
$m_{RG} = 0.666$	0	5	-2	5

Table 12: EbN0 (dB) Needed to achieve a fixed Pacq (NO RG Cancellation)

	$B \cdot T_b = 0.25$, T_4B		$B \cdot T_b = 0.50$, T_4B	
P_{ACQ}	1%	100%	1%	100%
$m_{RG} = 0.111$	14	23	12	21
$m_{RG} = 0.222$	7	15	5	15
$m_{RG} = 0.444$	2	9	1	8
$m_{RG} = 0.666$	0	5	-3	5

As for the detection of Ranging, both with RG Cancellation and without, there is no clear improvement pattern. We can deduce that the RG Cancellation is absolutely focused on the improvement in telemetry reception, in addition to not having any inconvenience that deteriorates the ranging system in principle.

5. Conclusions and Future Developments

In the present project, a reception system has been presented for the downlink proposed by the standard CCSDS to stop the rapid saturation of the frequency bands assigned to deep-space missions.

The main objective of this project is to verify and demonstrate the functionality of the reception system as well as to study the limiting factors necessary to compensate.

The results obtained in the first place have been quite satisfactory in the frequency domain, highlighting the spectral versatility that GMSK modulation provides. Even so, as far as detection is concerned, it has been seen how the ranging could imply a great deterioration in the system and therefore the range of parameters to be chosen was diminished.

To solve the problems found on this front, a new recommendation is applied based on the cancellation of ranging to reduce the impact of the ranging especially for high modulation rates.

As it is verified, the results obtained were suitable for any possible combination between **time-bandwidth product** and **modulation indices** and therefore the range of parameters to choose is not limited as in the previous case even taking into account the worst case. Therefore, we achieve a great frequency and error probability performance, hence, it is concluded that the requirements are met on the main fronts.

In addition, an appropriate parameter choice according to the type of mission, classified according to CCSDS as Category A and B would be the one shown in the following table:

Table 13: Recommended Parameters according to results and CCSDS

Mission Category According CCSDS	**Recommended Ranging Parameters**	**Recommended Telemetry Parameters**
Category A	**Ranging:** Regenerative PN T2B and T4B Sinewave shaping. m_{RG} between 0.2 and 0.45 rad.	**Telemetry:** GMSK *BT*s=0.25. **PN ranging chip rate to telemetry symbol rate:** Ratio higher than 1 (non-integer). $\frac{R_{RG}}{R_{TM}} \geq 1$
Category B	**Ranging:** Regenerative PN T2B and T4B Sinewave shaping. m_{RG} between 0.2 and 0.45 rad.	**Telemetry:** GMSK *BT*s=0.50. **PN ranging chip rate to telemetry symbol rate:** ratio higher than 1 (non-integer). $\frac{R_{RG}}{R_{TM}} \geq 1$

This choice of parameters based on the results obtained during the project allows a satisfactory performance in terms of the factors studied although there are many effects that should be taken into account to make a much more precise choice.

Future Development and Improvements

Regarding future developments and improvements, it would be interesting and necessary to study other effects that could adversely affect the system. These could be, doppler, asynchronization, clock drift and other negative impacts caused by space environment.

Then, a physical implementation of the project should be developed, that is, develop the hardware and see what effects and technological degradation can appear as jitter etc.

An important objective would be to reduce the computational cost of certain blocks of the system, mainly on the telemetry reception such as developing a fast Viterbi Algorithm.

On the other hand, an improvement in the system would be the development of an alternative to the bank of correlators that conforms the ranging receive block more compact and robust.

6. Budget

The work to develop the project has basically consisted of code development, simulations and understanding of the theoretical bases and technics that make it up and that constitute it.

Therefore, no prototype (hardware) has been developed.

Moreover, the equipment has consisted mainly on a Laptop with enough characteristic to run simulations in a decent range of time with MATLAB software. Although the project has last for approximately 5 months (September to January), no monthly MATLAB licenses are available, so the real cost of the software results in an annual license of **2.000 €.** (The cost given is for a real scenario, in this case a student license has been used).

In a common company, a laptop with those characteristics would last for 3 years and taking into account that the original cost of the computer is about **1.000 €,** the proportional part of the cost for this project is $\mathbf{138.8}$ **€.**

$$\frac{5\ months}{36\ months} * 1000\ € = 138.8\ €$$

On the other hand, taking into account that work time invested through the project was estimated to be about 450 hours and that the salary per hour of a junior engineer is around 12.5 €/hour, the total salary for the student would be **5.625** €.

Item	Cost
MATLAB License	**2.000** €
HP Laptop	**138.8** €
Hours Dedicated	**5.625** €
Total	**7763,8** €

Bibliography:

[1] Consultative Committee for Space Data Systems. (2019). Radio Frequency and Modulation Systems — Part 1 Earth Stations and Spacecraft. Blue Book, 401.0-B-29(29). Retrieved from https://public.ccsds.org/Pubs/401x0b29.pdf

[2] ECSS-E-ST-50-05-C, "Radio frequency and modulation", October 2011. - https://ecss.nl/standard/ecss-e-st-50-05c-rev2-radio-frequency-and-modulation-4-october-2011/

[3] CCSDS 413.1-G-1, Simultaneous transmission of GMSK telemetry and PN ranging greenbook, May 2017, https://public.ccsds.org/Pubs/413x1g1.pdf

[4] Pseudo-Noise (PN) ranging systems - recommended standard, CCSDS 414.1-B-2, February 2014, https://public.ccsds.org/Pubs/414x1b2.pdf

[5] ITU-R. (2009). Factors affecting the choice of frequency bands for space research service deep-space (space-to-Earth) telecommunication links. Report ITU-R SA.2167, 2167. Retrieved from http://www.itu.int/dms_pub/itu-r/opb/rep/R-REP-SA.2167-2009-PDF-E.pdf

[6] Rey, F., & Tarrés, F. (n.d.). Modulacions digitals de fase contínua (CPM).

[7] Simon, M. K., Lee, D., Martin, W. L., Tsou, H., & Yan, T.-Y. (2005). Bandwidth-Efficient Digital Modulation with Application to Deep Space Communications. Bandwidth-Efficient Digital Modulation with Application to Deep Space Communications. https://doi.org/10.1002/0471728500

[8] Kaleh, G. K. (1989). Simple Coherent Receivers for Partial Response Continuous Phase Modulation. IEEE Journal on Selected Areas in Communications, 7(9), 1427–1436. https://doi.org/10.1109/49.44586

[9] Tsou, T. (2012). On the Linear Representation of GMSK Modulation.

[10] RANGING SYSTEMS Greenbook. (2014), (February). https://public.ccsds.org/Pubs/414x0g2.pdf

[11] Kinman, P. W. (2004). Pseudo-noise and regenerative ranging. DSMS Telecommunications Link Design Handbook (810-005, Rev. E), (1), 1–36. Retrieved from http://scholar.google.com/scholar?hl=en&btnG=Search&q=intitle:Pseudo-Noise+and+Regenerative+Ranging#4

[12] Pseudo-Noise (PN) ranging systems - recommended standard, CCSDS 414.1-B-2, February 2014, Bluebook https://public.ccsds.org/Pubs/414x0g2.pdf

[13] Murota, K., & Hirade, K. (1981). GMSK Modulation for Digital Mobile Radio Telephony. IEEE Transactions on Communications, 29(7), 1044–1050. https://doi.org/10.1109/TCOM.1981.1095089

[14] Ku, Y. H., & Sun, X. (1992). The chinese remainder theorem. Journal of the Franklin Institute, 329(1), 93–97. https://doi.org/10.1016/0016-0032(92)90099-3

[15] Ding, C., Pei, D., & Salomaa, A. (2010). Chinese Remainder Theorem. In Chinese Remainder Theorem. https://doi.org/10.1142/9789812779380

Glossary

TM, Telemetry

RG, Ranging

CCSDS, Consultative Committee for Space Data Systems

PN, Pseudo-Noise

GMSK, Gaussian Minimum Shift Keying

ECSS, European Cooperation for Space Standardization

BER, Bit Error Rate

VA, Viterbi Algorithm

SFCG, Space Frequency Coordination Group

CPM, Continuous Phase Modulation

FM, Frequency Modulation

SNR, Signal to Noise Ratio

PSD, Power Spectral Density

AMP, Amplitude Modulation Pulse